static water contact angle on the Co–Cr–Mo surface before the MPC grafting was approximately 70°–90°; however, among the three differently pretreated surfaces, the nitric acid- and O_2 plasma-pretreated Co–Cr–Mo-*g*-MPC surface showed the lowest angle. The static water contact angle on the nitric acid- and O_2 plasma-pretreated Co–Cr–Mo-*g*-MPC surface was as low as 15°. On the other hand, compared to the angle on the untreated Co–Cr–Mo surface, the angle on the only nitric acid-pretreated Co–Cr–Mo-*g*-MPC surface was almost unchanged (approximately 65°) and that on the only O_2 plasma-pretreated Co–Cr–Mo-*g*-MPC surface was slightly decreased to 45°.

Fig. 6 shows the FM images of the untreated Co–Cr–Mo surface and the nitric acid- and O_2 plasma-pretreated Co–Cr–Mo-*g*-MPC surface. On the Co–Cr–Mo-*g*-MPC surface, rhodamine 6G stained poly(MPC) selectively (Fig. 6(b)). This resulted in a large contrast in the fluorescence intensity between the MPC-grafted layer (green–yellow) and the non-grafted substrates (blue) (Fig. 6(d)). The poly(MPC) layer stained with rhodamine 6G was more clearly visible but the staining was not uniform. It therefore indicates that the grafting of the poly(MPC) layer on the Co–Cr–Mo surface is not uniform. On the untreated Co–Cr–Mo surface, such a contrast was not observed (Fig. 6(a) and (c)).

Fig. 7 shows the friction coefficients of the sliding couples, namely, Co–Cr–Mo-*g*-MPC, CLPE, CLPE-*g*-MPC, and untreated Co–Cr–Mo pins sliding against the Co–Cr–Mo-*g*-MPC and untreated Co–Cr–Mo plates. The Co–Cr–Mo/Co–Cr–Mo couple showed a high friction coefficient of approximately 0.24 in the initial 10 cycles; the value increased gradually and reached approximately 0.38 after 5.0×10^4 cycles. The CLPE/Co–Cr–Mo-*g*-MPC and Co–Cr–Mo/Co–Cr–Mo-*g*-MPC couples showed a lower friction coefficient than the CLPE/untreated Co–Cr–Mo and Co–Cr–Mo/untreated Co–Cr–Mo couples, respectively. The CLPE/Co–Cr–Mo-*g*-MPC couple showed the lowest friction coefficient of approximately 0.05, and this value was almost steady during the experiment. In both CLPE-*g*-MPC/Co–Cr–Mo-*g*-MPC and Co–Cr–Mo-*g*-MPC/Co–Cr–Mo-*g*-MPC couples, the poly(MPC) layer sliding against the MPC polymer layer showed almost the same friction coefficient of approximately 0.12 up to the initial 100 cycles. After 5.0×10^4 cycles, the friction coefficients of the Co–Cr–Mo/Co–Cr–Mo-*g*-MPC and Co–Cr–Mo-*g*-MPC/Co–Cr–Mo-*g*-MPC couples increased, whereas that of the CLPE-*g*-MPC/Co–Cr–Mo-*g*-MPC couple decreased.

4. Discussion

In this study, with the aim of reducing wear, we synthesized a high lubricious Co–Cr–Mo alloy surface by poly(MPC) grafting for its application in artificial joints. To ensure the in vivo long-term retention of this

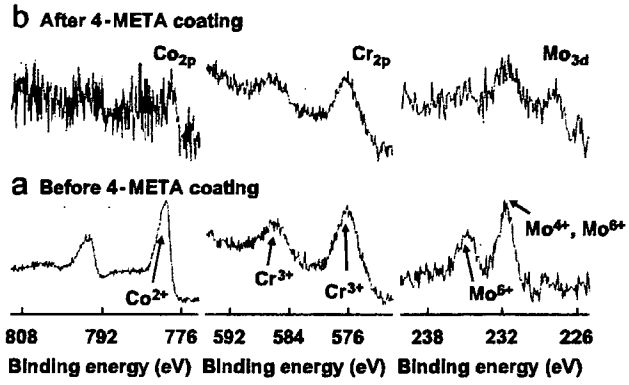

Fig. 3. XPS spectra of the binding energy region of the Co_{2p}, Cr_{2p}, and Mo_{3d} electrons from the nitric acid- and O_2 plasma-pretreated Co Cr Mo samples (a) before and (b) after the 4-META coating.

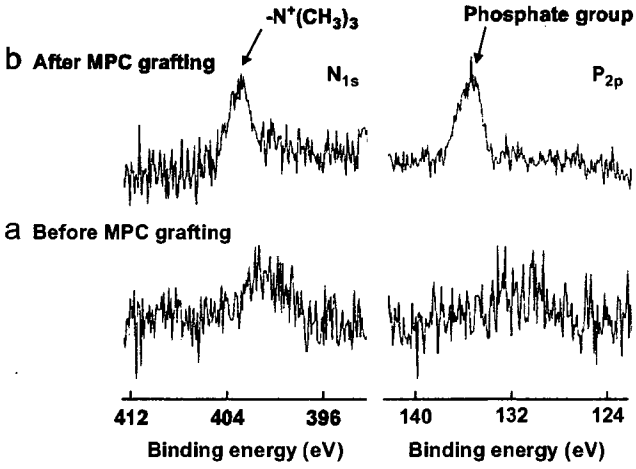

Fig. 4. XPS spectra (N_{1s} and P_{2p}) of the (a) untreated Co Cr Mo and (b) nitric acid- and O_2 plasma-pretreated Co Cr Mo-*g*-MPC samples.

Table 2
Surface elemental composition (%) of the pretreated Co Cr Mo alloy before MPC graft polymerization

Pretreatment	C_{1s}	O_{1s}	N_{1s}	P_{2p}	Co_{2p}	Cr_{2p}	Mo_{3d}
Untreated	44.2 (5.1)	39.3 (2.8)	0.6 (0.2)	0.0 (0.0)	10.5 (2.5)	4.5 (0.5)	1.0 (0.2)
Nitric acid	29.6 (3.8)	37.3 (1.6)	0.4 (0.8)	0.0 (0.0)	9.4 (0.7)	21.3 (2.1)	2.1 (0.2)
O_2 plasma	13.9 (0.5)	53.5 (0.9)	0.0 (0.0)	0.0 (0.0)	30.5 (1.2)	1.8 (0.5)	0.3 (0.1)
Nitric acid + O_2 plasma	14.6 (1.3)	52.9 (2.7)	0.0 (0.0)	0.0 (0.0)	26.7 (1.5)	5.4 (0.2)	0.4 (0.0)

$n = 5$.
The standard deviations are shown in parentheses.

Table 3
Surface elemental composition (%) of the Co Cr Mo-*g*-MPC samples that were subjected to different types of pretreatments

Pretreatment	MPC treatment	C_{1s}	O_{1s}	N_{1s}	P_{2p}	Co_{2p}	Cr_{2p}	Mo_{3d}
Nitric acid + O_2 plasma	Untreated	14.6 (1.3)	52.9 (2.7)	0.0 (0.0)	0.0 (0.0)	26.7 (1.5)	5.4 (0.2)	0.4 (0.0)
Untreated	MPC treatment	52.3 (1.3)	35.3 (0.4)	0.3 (0.2)	0.9 (0.1)	4.8 (0.8)	5.6 (1.1)	0.8 (0.1)
Nitric acid	MPC treatment	52.1 (1.1)	36.2 (0.7)	0.4 (0.2)	1.6 (0.2)	3.4 (0.4)	5.7 (0.7)	0.7 (0.2)
O_2 plasma	MPC treatment	42.1 (1.1)	45.6 (1.1)	0.2 (0.2)	1.0 (0.1)	10.5 (0.7)	0.4 (0.5)	0.2 (0.1)
Nitric acid + O_2 plasma	MPC treatment	63.3 (0.6)	30.8 (0.7)	3.0 (0.2)	2.9 (0.1)	0.0 (0.0)	0.0 (0.0)	0.0 (0.0)
MPC polymer*	MPC treatment	57.9	31.6	5.3	5.3	—	—	—

$n = 5$.
*Theoretical elemental composition of MPC polymer. The standard deviations are shown in parentheses.

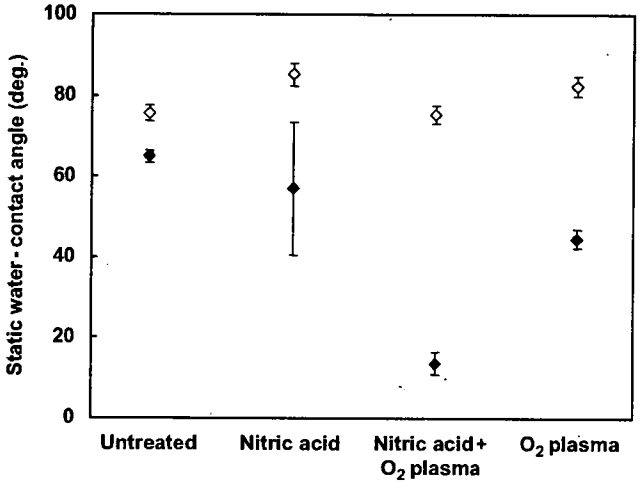

Fig. 5. Static water contact angle on the Co Cr Mo surfaces that were subjected to different types of pretreatments before and after the MPC grafting. Open marks, before MPC grafting; closed marks, after MPC grafting.

poly(MPC) graft on the Co–Cr–Mo alloy, we used the 4-META intermediate layer and the photo-induced radical graft polymerization technique to create a strong bonding between the Co–Cr–Mo substrate and the poly(MPC) chain via the 4-META layer. 4-META has already been known as a binder used in dental resin, and it can strongly bind resin to metal in dental implants [41,42]. Suzuki et al. [49] reported a strong evidence that the carboxylate anions were formed due to an ionic interaction between the carboxyl group of poly(carbonic acid) and the surface hydroxyl group on the oxide layer of stainless steel. Yamabe [50] reported that an ionic bond was formed between the carboxyl group and Cr on the surface of stainless steel. The various pretreatments performed in this study aimed at an efficient interaction between the carboxyl group of the 4-META layer and the surface hydroxyl group on the Cr oxide layer of the Co–Cr–Mo alloy.

As presented in Table 2, the surface Cr content in the Co–Cr–Mo alloy after the nitric acid pretreatment was higher than that of the untreated Co–Cr–Mo alloy. Seo and Sato [39] reported that a dry-polished stainless steel lacked in the surface Cr content. Accordingly, the as-polished Co–Cr–Mo alloy in this study may also lack the surface Cr content, and the surface etching by nitric acid treatment would have produced the Cr-rich surface layer.

Exposure of the Co–Cr–Mo alloy to O_2 plasma formed an oxide layer on the Co–Cr–Mo surface (Table 2 and Fig. 3(a)). The static water contact angle on the nitric acid-pretreated Co–Cr–Mo-*g*-MPC surface was higher than that on the nitric acid- and O_2 plasma-pretreated Co–Cr–Mo-*g*-MPC surface (Fig. 5). Additionally, the measured compositions of N and P in the only nitric acid-pretreated Co–Cr–Mo-*g*-MPC samples were lower than those in the nitric acid- and O_2 plasma-pretreated Co–Cr–Mo-*g*-MPC samples (Table 3). It was considered that washing with ethanol removed the 4-META-MPC graft copolymer (4-META-*co*-MPC) from the only nitric acid-pretreated Co–Cr–Mo surface because there was an inadequate ionic bonding between 4-META and the only nitric acid-pretreated Co–Cr–Mo surface without an oxide layer.

The peaks at 780, 236, and 232 eV in the XPS spectra were assigned to Co^{2+}, Mo^{4+}, and Mo^{6+}, respectively, as shown in Fig. 3. After the 4-META coating, these peaks disappeared from the Co–Cr–Mo surface. The peaks at 586 and 576 eV in the XPS spectra were assigned to Cr^{3+} (Fig. 3), indicating that Cr^{3+} persisted on the Co–Cr–Mo surface even after the 4-META coating. These results suggest that compared to other metallic oxides, Cr^{3+} predominantly binds to the carboxyl group of 4-META with a stronger ionic interaction [50]. This can be explained by the Lewis acid–base interaction model of a previous study [50]. It is assumed that the proton exchange between the carboxyl groups and active electrophilic metallic ions existing in the surface-hydrated oxide resulted in the formation of carboxylate anions; these carboxyl species that diffused into the hydrated oxide layer could easily undergo strong ionic interactions with the polar hydroxyl groups of hydrated Cr^{3+}. The binding between 4-META-*co*-MPC and the Co–Cr–Mo substrate might contribute to the stable polymer/metal interface.

Friction coefficients of various bearing couples in the previous studies are summarized in Table 4. In Fig. 7, the Co–Cr–Mo/Co–Cr–Mo couple showed a friction coefficient of approximately 0.24 as high as the previous studies. The CLPE/Co–Cr–Mo couple also showed a friction coefficient of approximately 0.09 as high as the previous studies. In contrast, it was confirmed that compared to the

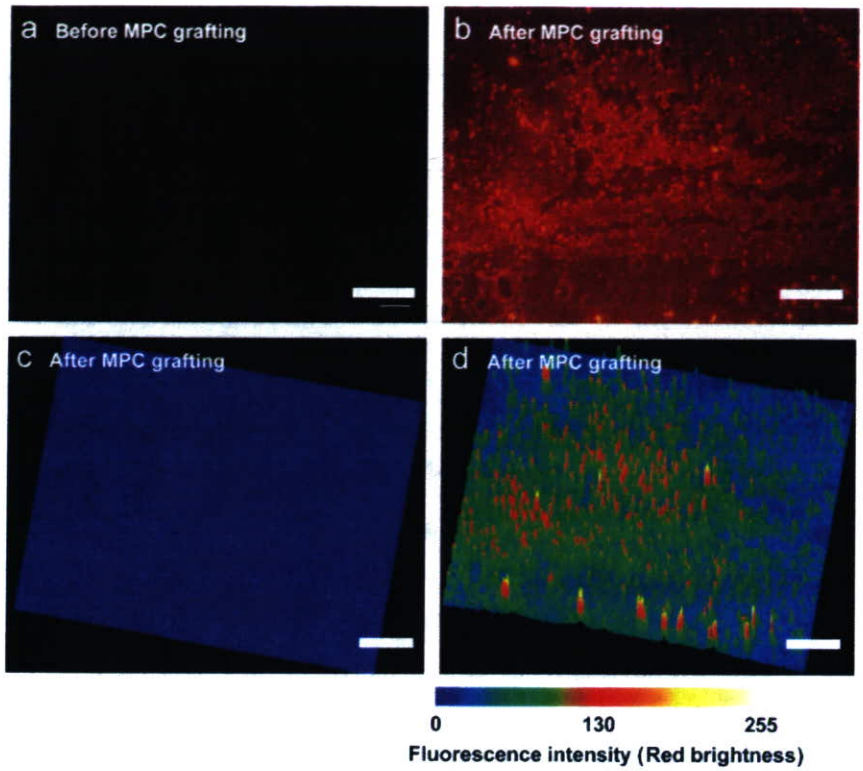

Fig. 6. FM images of (a), (c) the untreated Co Cr Mo and (b), (d) the nitric acid- and O_2 plasma-pretreated Co Cr Mo-*g*-MPC samples. (a and b) = FM images; (c and d) = color images from fluorescence intensity of the FM images (a and b). Bar = 200 μm. Color scale bar indicates fluorescence intensity (red brightness) for (c and d).

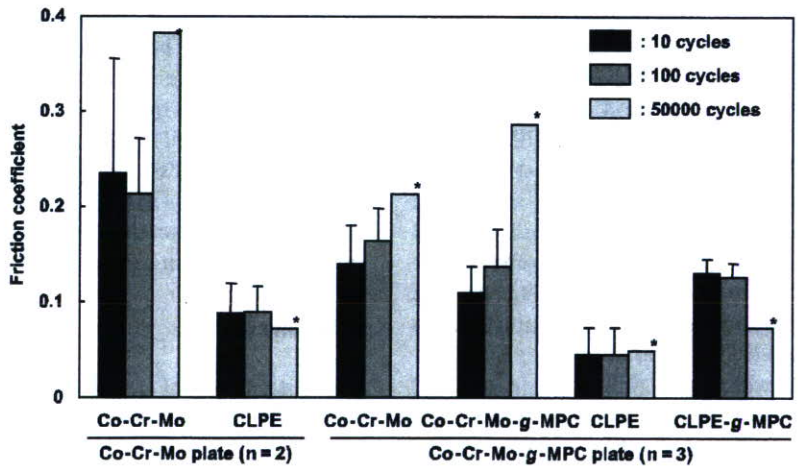

Fig. 7. Friction coefficients as a function of the test duration for the various types of pins sliding against the Co Cr Mo-*g*-MPC ($n = 3$) and untreated Co Cr Mo ($n = 2$) plates. *$n = 1$. Bars = standard deviations.

untreated Co–Cr–Mo surface, the Co–Cr–Mo-*g*-MPC (excluding the CLPE-*g*-MPC/Co–Cr–Mo-*g*-MPC-bearing couple) surface showed an extremely low friction coefficient. Since MPC is highly hydrophilic and poly(MPC) is water soluble, the water wettability of the Co–Cr–Mo-*g*-MPC surface was greater than that of the untreated Co–Cr–Mo surface, as shown in Fig. 5. Consequently, the grafted poly(MPC) layer successfully provided high lubricity to the Co–Cr–Mo surface (Fig. 7). The reduction in the friction may contribute to the improvement in the anti-wear properties [22]. From the viewpoint of tribological advantage, a highly lubricious metal-bearing material will enable the development of a novel biocompatible artificial hip-joint system.

Various factors such as the type of bearing material, surface roughness, homogeneity of the surface, and chemical composition affect the lubricity of artificial joints [54]. In the case of Co–Cr–Mo-*g*-MPC, the lubricity would

Table 4
Friction coefficients of various bearing couples in the previous studies

Bearing couple		Friction coefficient	References
Pin	Disc or plate		
Co Cr Mo	Co Cr Mo	0.19 0.27	[51]
UHMWPE	Co Cr Mo	0.05 0.09	[52]
UHMWPE	Co Cr Mo	0.05 0.09	[53]
Cartilage	Stainless steel	0.01 0.05	[55]
Cartilage	Cartilage	0.02	[56]

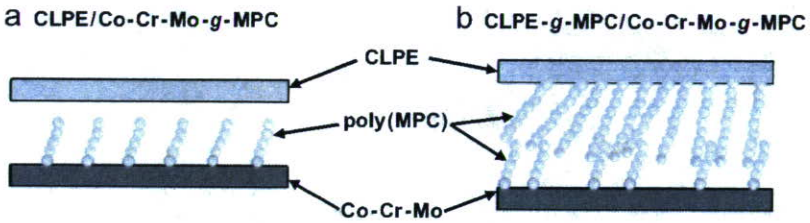

Fig. 8. Images of grafted non-grafted poly(MPC)/grafted poly(MPC) and poly(MPC)/grafted poly(MPC)-bearing interfaces.

change depending on the ambient in vitro and in vivo conditions. The bearing surface with poly(MPC) in artificial hip joints is assumed to have a structure similar to an artificial cell membrane. The Co–Cr–Mo-*g*-MPC/Co–Cr–Mo-*g*-MPC or CLPE-*g*-MPC/Co–Cr–Mo-*g*-MPC-bearing couples therefore mimic the natural joint cartilage in vivo. A friction coefficient of cartilage/SUS pin-on-plate was 0.01–0.05 [55], and that of cartilage/cartilage pin-on-plate was 0.02 [56], as shown in Table 4. In contrast, the Co–Cr–Mo-*g*-MPC/Co–Cr–Mo-*g*-MPC or CLPE-*g*-MPC/Co–Cr–Mo-*g*-MPC-bearing couples mimicking the natural joint, showed high friction (friction coefficient = 0.12) in this study. Images of grafted non-grafted poly(MPC)/grafted poly(MPC) and poly(MPC)/grafted poly(MPC)-bearing interfaces are shown in Fig. 8. The grafted poly(MPC)/non-grafted poly(MPC)-bearing interface in the CLPE/Co–Cr–Mo-*g*-MPC couple showed a low friction coefficient with the water wettability of poly(MPC) (Fig. 8(a)). The grafted poly(MPC)/grafted poly(MPC)-bearing interface in the CLPE-*g*-MPC/Co–Cr–Mo-*g*-MPC couple showed slightly higher friction than the grafted poly(MPC)/non-grafted poly(MPC)-bearing interface. The MPC graft polymer on Co–Cr–Mo might have low density because the polymerization method used was "grafting to" [57]. Fukuda et al. [58] reported that the friction was higher in a bearing couple with low-density polymer brushes than in a bearing couple with high-density polymer brushes. Therefore, it is assumed that a bearing couple with low-density poly(MPC) brushes may cause high friction with interpenetration as shown in Fig. 8(b) [59]. High-density poly(MPC) by "grafting from" might be possible to resist the interpenetration by its volume effects arising from chain mobility.

5. Conclusions

We created a highly lubricious metal-bearing material for its application as a novel artificial hip-joint system: The MPC polymer was grafted onto the surface of the Co–Cr–Mo alloy by employing the 4-META intermediate layer and using the photo-induced radical graft polymerization technique and the nitric acid and O_2 plasma pretreatments of the Co–Cr–Mo alloy. In conclusion, the grafted poly(MPC) layer successfully provided high lubricity to the Co–Cr–Mo surface. The grafted poly(MPC)/non-grafted poly(MPC)-bearing interface had a lower friction value than that of the grafted poly(MPC)/grafted poly(MPC) bearing interface.

References

[1] Kurtz S, Mowat F, Ong K, Chan N, Lau E, Halpern M. Prevalence of primary and revision total hip and knee arthroplasty in the United States from 1990 through 2002. J Bone Joint Surg Am 2005;87(7):1487 97.
[2] Harris WH. The problem is osteolysis. Clin Orthop 1995;311:46 53.
[3] Kobayashi A, Freeman MA, Bonfield W, Kadoya Y, Yamac T, Al-Saffar N, et al. Number of polyethylene particles and osteolysis in total joint replacements. A quantitative study using a tissue-digestion method. J Bone Joint Surg Br 1997;79(5):844 8.
[4] Sochart DH. Relationship of acetabular wear to osteolysis and loosening in total hip arthroplasty. Clin Orthop 1999;363:135 50.
[5] McKellop H, Shen FW, Lu B, Campbell P, Salovey R. Development of an extremely wear-resistant ultra high molecular weight polyethylene for total hip replacements. J Orthop Res 1999;17(2):157 67.
[6] Muratoglu OK, Bragdon CR, O'Connor DO, Jasty M, Harris WH. A novel method of crosslinking ultra-high-molecular-weight polyethylene to improve wear, reduce oxidation, and retain mechanical properties: recipient of the 1999 HAP Paul Award. J Arthroplasty 2001;16(2):149 60.

[7] Urban JA, Garvin KL, Boese CK, Bryson L, Pedersen DR, Callaghan JJ, et al. Ceramic-on-polyethylene bearing surfaces in total hip arthroplasty. Seventeen to twenty-one-year results. J Bone Joint Surg Am 2001;83(11):1688 94.
[8] St John KR, Zardiackas LD, Poggie RA. Wear evaluation of cobalt chromium alloy for use in a metal-on-metal hip prosthesis. J Biomed Mater Res B Appl Biomater 2004;68(1):1 14.
[9] McMinn DJ, Daniel J, Pynsent PB, Pradhan C. Mini-incision resurfacing arthroplasty of hip through the posterior approach. Clin Orthop Relat Res 2005;441:91 8.
[10] Clarke IC, Good V, Williams P, Schroeder D, Anissian L, Stark A, et al. Ultra-low wear rates for rigid-on-rigid bearings in total hip replacements. Proc Inst Mech Eng [H] 2000;214(4):331 47.
[11] Fisher J, Hu XQ, Stewart TD, Williams S, Tipper JL, Ingham E, et al. Wear of surface engineered metal-on-metal hip prostheses. J Mater Sci Mater Med 2004;15(3):225 35.
[12] Keel JB, Kuster MS. Massive wear of an incompatible metal-on-metal articulation in total hip arthroplasty. J Arthroplasty 2004;19(5):638 42.
[13] Korovessis P, Petsinis G, Repanti M, Repantis T. Metallosis after contemporary metal-on-metal total hip arthroplasty. Five to nine-year follow-up. J Bone Joint Surg Am 2006;88(6):1183 91.
[14] Savarino L, Granchi D, Ciapetti G, Cenni E, Nardi Pantoli A, Rotini R, et al. Ion release in patients with metal-on-metal hip bearings in total joint replacement: a comparison with metal-on-polyethylene bearings. J Biomed Mater Res 2002;63(5):467 74.
[15] Dowson D, Hardaker C, Flett M, Isaac GH. A hip joint simulator study of the performance of metal-on-metal joints: Part I: the role of materials. J Arthroplasty 2004;19(8):118 23.
[16] Bowsher JG, Nevelos J, Williams PA, Shelton JC. 'Severe' wear challenge to 'as-cast' and 'double heat-treated' large-diameter metal-on-metal hip bearings. Proc Inst Mech Eng [H] 2006;220(2):135 43.
[17] Brizuela M, Garcia-Luis A, Viviente JL, Braceras I, Onate JI. Tribological study of lubricious DLC biocompatible coatings. J Mater Sci Mater Med 2002;13(12):1129 33.
[18] Gutmanas EY, Gotman I. PIRAC Ti nitride coated Ti-6AI-4V head against UHMWPE acetabular cup-hip wear simulator study. J Mater Sci Mater Med 2004;15(4):327 30.
[19] Bowsher JG, Hussain A, Williams P, Nevelos J, Shelton JC. Effect of ion implantation on the tribology of metal-on-metal hip prostheses. J Arthroplasty 2004;19(8):107 11.
[20] Oka M, Ushio K, Kumar P, Ikeuchi K, Hyon SH, Nakamura T, et al. Development of artificial articular cartilage. Proc Inst Mech Eng [H] 2000;214(1):59 68.
[21] Ushio K, Oka M, Hyon SH, Yura S, Toguchida J, Nakamura T. Partial hemiarthroplasty for the treatment of osteonecrosis of the femoral head. An experimental study in the dog. J Bone Joint Surg Br 2003;85(6):922 30.
[22] Moro T, Takatori Y, Ishihara K, Konno T, Takigawa Y, Matsushita T, et al. Surface grafting of artificial joints with a biocompatible polymer for preventing periprosthetic osteolysis. Nat Mater 2004;3:829 37.
[23] Kyomoto M, Moro T, Konno T, Takadama H, Yamawaki N, Kawaguchi H, et al. Enhanced wear resistance of modified cross-linked polyethylene by grafting with poly(2-methacryloyloxyethyl phosphorylcholine). J Biomed Mater Res A, forthcoming.
[24] Kyomoto M, Moro T, Konno T, Takadama H, Kawaguchi H, Takatori Y, et al. Effects of photo-induced graft polymerization of 2-methacryloyloxyethyl phosphorylcholine on physical properties of cross-linked polyethylene in artificial hip joints. J Mater Sci Mater Med, forthcoming.
[25] Ishihara K, Ueda T, Nakabayashi N. Preparation of phospholipid polymers and their properties as polymer hydrogel membranes. Polym J 1990;22(5):355 60.
[26] Ishihara K, Aragaki R, Ueda T, Watanabe A, Nakabayashi N. Reduced thrombogenicity of polymers having phospholipid polar groups. J Biomed Mater Res 1990;24:1069 77.
[27] Ishihara K, Ziats NP, Tierney BP, Nakabayashi N, Anderson JM. Protein adsorption from human plasma is reduced on phospholipids polymers. J Biomed Mater Res 1991;25(11):1397 407.
[28] Goda T, Konno T, Takai M, Moro T, Ishihara K. Biomimetic phosphorylcholine polymer grafting from polydimethylsiloxane surface using photo-induced polymerization. Biomaterials 2006;27(30): 5151 60.
[29] Sibarani J, Takai M, Ishihara K. Surface modification on microfluidic devices with 2-methacryloyloxyethyl phosphorylcholine polymers for reducing unfavorable protein adsorption. Colloids Surf B Biointerfaces 2007;54(1):88 93.
[30] Ueda H, Watanabe J, Konno T, Takai M, Saito A, Ishihara K. Asymmetrically functional surface properties on biocompatible phospholipid polymer membrane for bioartificial kidney. J Biomed Mater Res A 2006;77(1):19 27.
[31] Abraham S, Brahim S, Ishihara K, Guiseppi-Elie A. Molecularly engineered p(HEMA)-based hydrogels for implant biochip biocompatibility. Biomaterials 2005;26(23):4767 78.
[32] Konno T, Hasuda H, Ishihara K, Ito Y. Photo-immobilization of a phospholipid polymer for surface modification. Biomaterials 2005;26(12):1381 8.
[33] Palmer RR, Lewis AL, Kirkwood LC, Rose SF, Lloyd AW, Vick TA, et al. Biological evaluation and drug delivery application of cationically modified phospholipid polymers. Biomaterials 2004;25(19):4785 96.
[34] Snyder TA, Tsukui H, Kihara S, Akimoto T, Litwak KN, Kameneva MV, et al. Preclinical biocompatibility assessment of the EVA-HEART ventricular assist device: coating comparison and platelet activation. J Biomed Mater Res A 2007;81(1):85 92.
[35] Kuiper KJ, Nordrehaug JE. Early mobilization after protamine reversal of heparin following implantation of phosphorylcholine-coated stents in totally occluded coronary arteries. Am J Cardiol 2000;85:698 702.
[36] Galli M, Sommariva L, Prati F, Zerboni S, Politi A, Bonatti R, et al. Acute and mid-term results of phosphorylcholine-coated stents in primary coronary stenting for acute myocardial infarction. Cathet Cardiovasc Intervent 2001;53:182 7.
[37] ASTM F75-01: Standard specification for cobalt-28 chromium-6 molybdenum alloy casting and casting alloy for surgical implants (UNS R30075). In: Arendt SA, Bailey SJ, editors. Annual book of ASTM standards, vol. 13, 2004.
[38] ASTM F86-04: Standard practice for surface preparation and marking of metallic surgical implants. In: Arendt SA, Bailey SJ, editors. Annual book of ASTM standards, vol. 13, 2004.
[39] Seo M, Sato N. Differential composition profiles in depth of thin anodic oxide films on iron-chromium alloy. Surf Sci 1979;86:601 9.
[40] Ishihara K, Nakabayashi N. Adhesive bone cement both to bone and metals: 4-META in MMA initiated with tri-*n*-butyl borane. J Biomed Mater Res 1989;23(12):1475 82.
[41] Yoshida K, Greener EH. Effects of coupling agents on mechanical properties of metal oxide-polymethacrylate composites. J Dent 1994;22(1):57 62.
[42] Givan DA, Fitchie JG, Anderson L, Zardiackas LD. Tensile fatigue of 4-META cement bonding three base metal alloys to enamel and comparison to other resin cements. J Prosthet Dent 1995;73(4): 377 85.
[43] Bryant SJ, Nuttelman CR, Anseth KS. Cytocompatibility of UV and visible light photoinitiating systems on cultured NIH/3T3 fibroblasts in vitro. J Biomater Sci Polym Ed 2000;11(5):439 57.
[44] International Organization for Standardization 15989: Plastics—film and sheeting—measurement of water-contact angle of corona-treated films, 2004.
[45] Wang JH, Bartlett JD, Dunn AC, Small S, Willis SL, Driver MJ, et al. The use of rhodamine 6G and fluorescence microscopy in the evaluation of phospholipid-based polymeric biomaterials. J Microsc 2005;217(Pt 3):216 24.
[46] Kumar P, Oka M, Ikeuchi K, Shimizu K, Yamamuro T, Okumura H, et al. Low wear rate of UHMWPE against zirconia ceramic (Y-PSZ)

in comparison to alumina ceramic and SUS 316L alloy. J Biomed Mater Res 1991;25(7):813 28.
[47] ASTM F732-00: Standard test method for wear testing of polymeric materials used in total joint prostheses. In: Arendt SA, Bailey SJ, editors. Annual book of ASTM standards, vol. 13, 2004.
[48] International Organization for Standardization 14242-1: implants for surgery: wear of total hip-joint prostheses Part 1: loading and displacement parameters for wear-testing machines and corresponding environmental conditions for test, 2002.
[49] Suzuki T, Yuasa M, Sekine I, Yamabe H, Fujiwara T, Amano S. Investigation of the improvement of the adhesion durability of stainless steels in wet environment by surface treatment with polymer containing carboxyl groups. Shikizai 1998;71(12):746 54.
[50] Yamabe H. Stabilization of the polymer-metal interface. Progr Org Coating 1996;28:9 15.
[51] Saldívar-García AJ, Lopez HF. Microstructural effects on the wear resistance of wrought and as-cast Co Cr Mo C implant alloys. J Biomed Mater Res A 2005;74(2):269 74.
[52] Sheeja D, Tay BK, Nung LN. Tribological characterization of surface modified UHMWPE against DLC-coated Co Cr Mo. Surf Coat Technol 2005;190(2 3):231 7.
[53] Saikko V. Wear and friction properties of prosthetic joint materials evaluated on a reciprocating pin-on-flat apparatus. Wear 1993;166(2): 169 78.
[54] Ho SP, Nakabayashi N, Iwasaki Y, Boland T, LaBerge M. Frictional properties of poly(MPC-co-BMA) phospholipid polymer for catheter applications. Biomaterials 2003;24(28):5121 9.
[55] Naka MH, Morita Y, Ikeuchi K. Influence of proteoglycan contents and of tissue hydration on the frictional characteristics of articular cartilage. Proc Inst Mech Eng [H] 2005;219(3):175 82.
[56] Bell CJ, Ingham E, Fisher J. Influence of hyaluronic acid on the time-dependent friction response of articular cartilage under different conditions. Proc Inst Mech Eng [H] 2006;220(1):23 31.
[57] Iwata R, Suk-In P, Hoven VP, Takahara A, Akiyoshi K, Iwasaki Y. Control of nanobiointerfaces generated from well-defined biomimetic polymer brushes for protein and cell manipulations. Macromolecules 2004;5(6):2308 14.
[58] Yamamoto S, Ejaz M, Tsujii Y, Fukuda T. Surface interaction forces of well-defined, high-density polymer brushes studied by atomic force microscopy. 2. Effect of graft density. Macromolecules 2000;33(15): 5608 12.
[59] Raviv U, Glasson S, Kampf N, Gohy JF, Jérôme R, Klein J. Lubrication by charged polymers. Nature 2003;425:163 5.

EMBO
reports

scientific report

S100A1 and S100B, transcriptional targets of SOX trio, inhibit terminal differentiation of chondrocytes

Taku Saito[1], Toshiyuki Ikeda[2], Kozo Nakamura[1], Ung-il Chung[2] & Hiroshi Kawaguchi[1+]

[1]Department of Sensory and Motor System Medicine, Faculty of Medicine, and [2]Faculty of Medicine, Center for Disease Biology and Integrative Medicine, University of Tokyo, Bunkyo, Tokyo, Japan

Transcription factor SOX9 (sex-determining region Y-type high mobility group box 9) and its coactivators SOX5 and SOX6 (the SOX trio) induce early-stage chondrocyte differentiation and suppress its terminal stage. To identify possible targets of the SOX trio, we carried out a microarray analysis and identified S100A1 and S100B as possible target molecules. S100 protein expression was localized in late proliferative and pre-hypertrophic chondrocytes of the mouse growth plate. Overexpression of S100A1, S100B or their combination in cultured chondrogenic cells did not induce early differentiation, but suppressed hypertrophic differentiation and mineralization. Silencing of both S100A1 and S100B stimulated terminal differentiation and reversed the SOX-trio-mediated inhibition. Finally, luciferase reporter, electrophoretic mobility shift and chromatin immunoprecipitation analyses showed that transcription of both S100 proteins is induced by the SOX trio, and also identified their respective enhancer elements in the 5′-end flanking region. We conclude that S100A1 and S100B are transcriptional targets of the SOX trio and mediate its inhibition of terminal differentiation of chondrocytes.

Keywords: SOX; S100; chondrocyte; cartilage; hypertrophy

EMBO reports (2007) **8**, 504–509. doi:10.1038/sj.embor.7400934

INTRODUCTION

During endochondral ossification for skeletal development, cells in the mesenchymal condensations differentiate into chondrocytes that then undergo proliferation and differentiation into hypertrophic cells. The hypertrophic chondrocytes mineralize a surrounding matrix to provide a scaffold for osteoblastic cells. Many lines of evidence have shown that the sex-determining region Y-type high mobility group box (SOX) family transcription factors are required at sequential steps of the chondrocyte differentiation (Bi *et al*, 2001; Akiyama *et al*, 2002). Among them, SOX9 is known to be an essential transcription factor for mesenchymal condensation and subsequent chondrocyte differentiation at an early stage (Foster *et al*, 1994; Wagner *et al*, 1994; Ng *et al*, 1997). Two members of the SOX family, SOX5 and SOX6, are known to function as coactivators of SOX9 in chondrocyte differentiation (Lefebvre *et al*, 1998; Smits *et al*, 2001). Accumulated evidence on mutant mice with loss of function of the SOX factors has shown that they also function as potent inhibitors of terminal differentiation (Bi *et al*, 2001; Smits *et al*, 2001; Akiyama *et al*, 2002). We reported previously that the combination of SOX9, SOX5 and SOX6 (the SOX trio) highly stimulated the early stage of chondrocyte differentiation in several cultured cells, including nonchondrogenic cells (Ikeda *et al*, 2004). In addition, the SOX trio inhibited terminal differentiation of chondrocytes. This effect could potentially be explored to benefit regenerative medicine of permanent cartilage. The present study sought to identify transcriptional targets of the SOX trio by a microarray analysis, and further investigated their functional involvement in chondrocyte differentiation.

[1]Department of Sensory and Motor System Medicine, Faculty of Medicine, and [2]Faculty of Medicine, Center for Disease Biology and Integrative Medicine, University of Tokyo, Hongo 7-3-1, Bunkyo, Tokyo 113-8655, Japan
[+]Corrresponding author. Tel: +81 33815 5411 ext. 30473; Fax: +81 33818 4082; E-mail: kawaguchi-ort@h.u-tokyo.ac.jp

Received 7 August 2006; revised 17 January 2007; accepted 29 January 2007; published online 30 March 2007

RESULTS AND DISCUSSION

Induction of S100A1 and S100B by the SOX trio

A microarray analysis was performed using human mesenchymal stem cells (hMSCs) adenovirally transfected with the SOX trio or a LacZ control. We identified 17 and 373 genes that were upregulated more than five- and twofold, respectively, as well as 5 and 230 genes downregulated more than five- and twofold, respectively, by the SOX trio (supplementary Table online). Among them, S100A1 and S100B—S100 protein family members, which are the largest subgroup in the superfamily of proteins carrying the Ca^{2+}-binding EF-hand motif—showed the strongest increases. Real-time reverse transcription–PCR (RT–PCR) analysis confirmed that S100A1 and S100B expression was induced by adenoviral transfection of SOX9 alone, and more strongly by that of the SOX trio—but not by SOX5 or SOX6 alone—in hMSCs, human dermal fibroblasts, chondrogenic cell line ATDC5 and nonchondrogenic cell lines HeLa and HuH-7 (Fig 1).

Expression patterns of S100A1 and S100B

To identify the expression patterns of S100A1 and S100B in the sequential differentiation stages of chondrocytes, we carried out

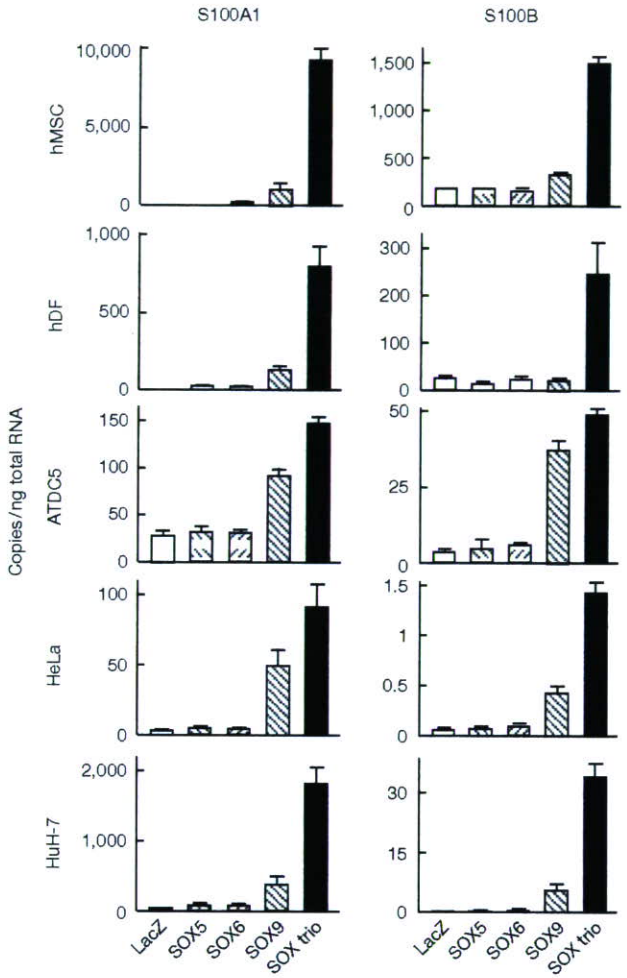

Fig 1 | Expression of S100A1 and S100B is induced by SOX9 and the SOX trio in cultures of human mesenchymal stem cells, human dermal fibroblasts, ATDC5, HeLa and HuH-7 cells. The cells were adenovirally transfected with LacZ, SOX5, SOX6, SOX9 or the SOX trio, and the messenger RNA levels were determined by real-time reverse transcription–PCR analysis after 7 days of culture. Data are shown as means (bars) ± s.d.s (error bars) for 4 wells/group. hDF, human dermal fibroblasts; hMSC, human mesenchymal stem cells; SOX, sex-determining region Y-type high mobility group box.

immunohistochemistry (Fig 2A) and *in situ* hybridization (supplementary Fig S1 online) in the mouse growth plate. S100A1 and S100B were coexpressed with SOX9, SOX5 and SOX6 in differentiated cells—late proliferative and pre-hypertrophic chondrocytes—and moderately in the hypertrophic chondrocytes. When their subcellular localization was examined by immunocytochemistry in cultured retrovirally transduced ATDC5 cells, both S100 proteins were localized in the cytoplasm (Fig 2B).

In cultured ATDC5 cells, expression of endogenous S100A1 and S100B was increased with expression of SOX9, SOX5 and SOX6, as well as type II collagen (COL2), type X collagen (COL10) and RUNX2 (runt-related transcription factor 2) during chondrogenic and hypertrophic differentiation (supplementary Fig S2 online).

Functional contribution of S100A1 and S100B

To investigate the functional relevance of S100A1 and S100B to chondrocyte differentiation, we first established stable lines of ATDC5 cells overexpressing S100A1, S100B, a combination of both or a green fluorescent protein (GFP) control through retroviral transduction. Gene expression was confirmed by real-time RT–PCR, western blot and immunofluorescence analyses (supplementary Fig S3A online). Both COL2 messenger RNA level and Alcian blue staining in the four different cell lines were comparable with those of non-transfected parental cells (supplementary Fig S3B online), indicating that the S100 proteins did not induce early differentiation of chondrocytes. Considering that the SOX trio not only induces early differentiation, but also suppresses terminal differentiation (Ikeda *et al*, 2004), we then examined the effects of the S100 proteins on ATDC5 cells that were cultured in differentiation medium including insulin and inorganic phosphate. The mRNA levels of terminal differentiation markers COL10 and RUNX2, alkaline phosphatase (ALP) activity and Alizarin red staining were reduced in cells overexpressing S100A1, S100B or a combination of both (Fig 3A).

Next, to investigate the effects of loss of function of S100A1 and S100B, we established stable lines of ATDC5 cells expressing small interfering RNA of S100A1, S100B, a combination of both or a GFP control, and confirmed the silencing of the genes (supplementary Fig S4A online). Although none of the early differentiation markers above was much affected (supplementary Fig S4B online), the terminal differentiation markers were markedly enhanced when both S100A1 and S100B were silenced (Fig 3B).

Adenoviral transfection of S100A1 + S100B suppressed COL10 expression similarly to expression of SOX9 or the SOX trio, and expression of SOX9 or the SOX trio induced S100A1 and S100B expression. These results indicate that the S100 proteins might mediate the inhibition of terminal differentiation by SOX signalling (Fig 3C). In fact, COL10 suppression by the SOX trio was not seen when S100A1 and S100B were silenced (Fig 3D). The recovery of COL10 by silencing the S100 proteins was reproducible in hMSCs (supplementary Fig S5 online).

Taking these data together, S100A1 and S100B are likely to mediate the suppression of terminal differentiation by the SOX trio, but seem not to be involved in induction of early chondrocyte differentiation.

Transcriptional induction of S100A1 and S100B

To examine the transcriptional regulation of S100A1, a luciferase-reporter gene construct containing a 1,000 bp fragment of the S100A1 5′-end flanking region was transfected into HeLa and HuH-7 cells. The transcriptional activity determined by the luciferase-reporter assay was enhanced by co-transfection with SOX9. Co-transfection of the SOX trio (but not of SOX5, SOX6 or the GFP control) further enhanced the transcriptional activity of the reporter (Fig 4A). Deletion analysis by a series of 5′-deletion constructs identified the core responsive element to SOX9 and the SOX trio to be between −135 and −95 region (A1 box). The tandem-repeat constructs of the A1 box responded to SOX9 and the SOX trio depending on its repeat number in both cell lines (Fig 4B). As this region contained paired SOX-binding motifs,

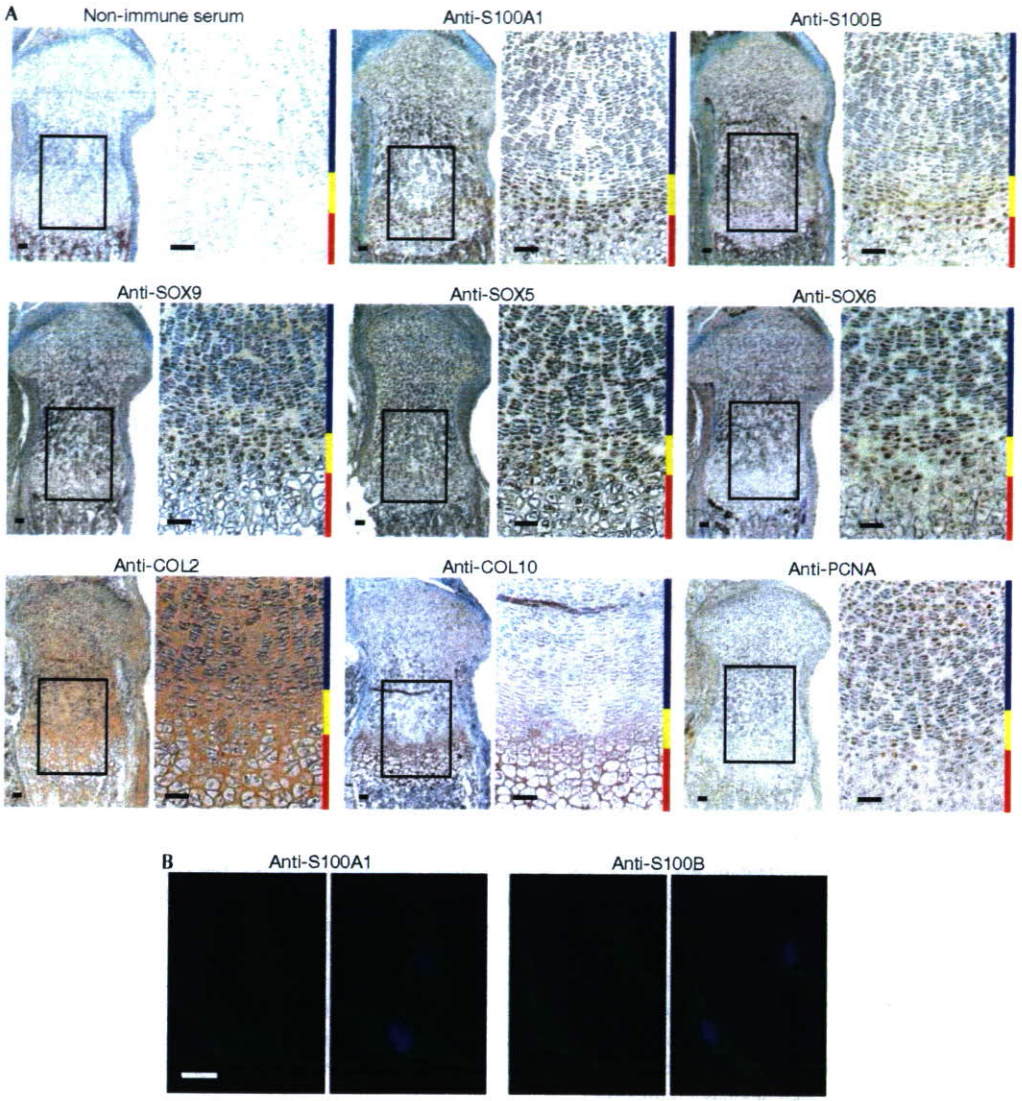

Fig 2 | S100A1 and S100B proteins are detected in late proliferative and pre-hypertrophic chondrocytes of the growth plate and localize in the cytoplasm of ATDC5 cells. (**A**) Localization of the S100 and SOX proteins was examined by immunohistochemistry in the fetal mouse growth plate and compared with that of COL2, COL10 and PCNA as early differentiation, hypertrophic differentiation and proliferation markers, respectively. Inset boxes in the left-hand figures indicate the regions of the respective right-hand figures. Scale bars, 50 μm. Blue, yellow and red bars at the right-hand side of each pair of figures indicate layers of proliferative, pre-hypertrophic and hypertrophic zones, respectively. (**B**) Subcellular localization was examined by immunocytochemistry in ATDC5 cells transfected with S100A1 (left) or S100B (right) with or without nuclear counterstaining. Scale bar, 10 μm. COL2, type II collagen; COL10, type X collagen; PCNA, proliferating cell nuclear antigen; SOX, sex-determining region Y-type high mobility group box.

surrounded by GC-rich sequences, site-directed mutagenesis of either or both of the motifs was carried out (m1, distal mutation; m2, proximal mutation; and m3, both mutations; Fig 4C, top panel). The transactivation abilities of SOX9 and the SOX trio were suppressed by m2 and m3, but not by m1, in the 1,000 bp fragment (Fig 4C, middle panel) and also in the four tandem-repeat constructs of A1 box (Fig 4C, bottom panel), indicating that the proximal motif is the core responsive element of SOX.

Electrophoretic mobility shift assay (EMSA) showed specific binding of *in vitro*-translated SOX9 with the wild-type and the m1 A1 box oligonucleotide probes, but not with the m2 or m3 probe (Fig 4D, left panel). Neither SOX5 nor SOX6 protein bound any of the oligonucleotide probes (data not shown). Cold competition with 50-fold excess of an unlabelled wild-type and m1 probe (but not with the unlabelled m2 or m3 probe) suppressed formation of the complex, confirming the specific

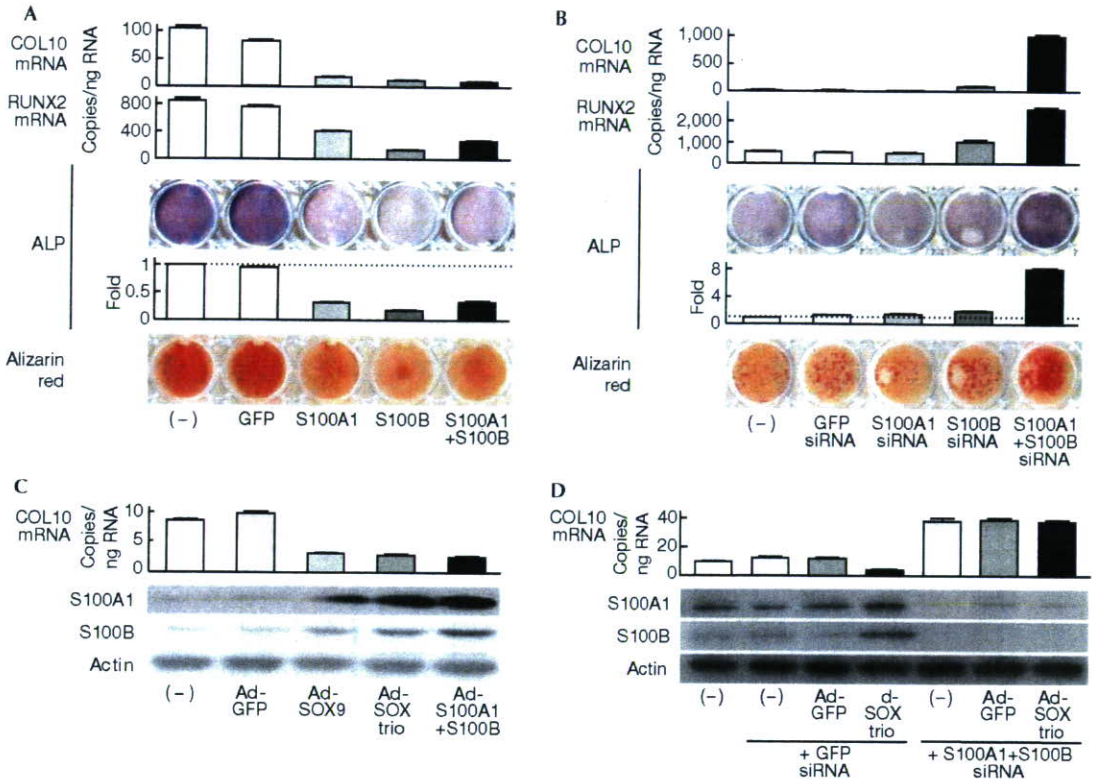

Fig 3 | S100A1 and S100B mediate the suppression of terminal differentiation of chondrocytes by the SOX trio. (**A**) Messenger RNA levels of the terminal differentiation markers COL10 and RUNX2, ALP staining and activity, and Alizarin red staining in stable lines of ATDC5 cells with retroviral transfection of GFP, S100A1, S100B or a combination of both, and in non-transfected parental cells (-) after culture for 3 weeks with ITS (insulin, transferrin and sodium selenite) and 2 days with inorganic phosphate. (**B**) Analysis of the above markers in stable lines of ATDC5 cells retrovirally transfected with siRNA of GFP, S100A1, S100B or a combination of both, and in non-transfected parental cells (-) under the culture conditions given above. (**C**) COL10 mRNA level and S100A1 and S100B protein levels are shown as western blots in ATDC5 cells with adenoviral transfection of GFP, SOX9, the SOX trio or S100A1 + S100B, and in non-transfected parental cells (-) after 10 days of a pellet culture. (**D**) Identical analysis in ATDC5 cells co-transfected with GFP or the SOX trio, and siRNA of GFP or S100A1 + S100B, compared with those in non-transfected parental cells (-) after 10 days of a pellet culture. The graphs are expressed as means (bars) ± s.d.s (error bars) for 3 wells/group. ALP, alkaline phosphatase; COL10, type X collagen; GFP, green fluorescent protein; PCNA, proliferating cell nuclear antigen; RUNX2, runt-related transcription factor 2; siRNA, small interfering RNA; SOX, sex-determining region Y-type high mobility group box.

binding of the proximal motif (Fig 4D, middle panel). Specificity of SOX9 binding was further verified by antibody supershift (Fig 4D, right panel).

Chromatin immunoprecipitation (ChIP) also showed binding of SOX9 to the S100A1 regulatory region including the A1 box in the presence or absence of SOX5 and SOX6 (Fig 4E). Specificity was confirmed as SOX9 because it was not immunoprecipitated by the non-immune IgG antibody (Fig 4F) and no amplification was seen with a primer set that does not span the A1 box (Fig 4G).

Similar assays were carried out to examine the transcriptional regulation of S100B by the SOX trio in HeLa and HuH-7 cells (supplementary Fig S6 online). Deletion, tandem-repeat and site-directed mutagenesis analyses of the luciferase-reporter assay indicated the transcriptional induction of S100B by the SOX trio and identified the core enhancer element of SOX9 between the −181 and −129 region in the 5′-end flanking region. EMSA and ChIP analyses also confirmed the specific binding of SOX9 to the enhancer motif.

Speculation

We conclude that S100A1 and S100B are transcriptional targets of the SOX trio and mediate its inhibition of terminal differentiation. This study identified, for the first time to our knowledge, SOX9 or SOX trio targets other than matrix proteins such as COL2 and aggrecan (Lefebvre *et al*, 1998; Sekiya *et al*, 2000). Interestingly, gain of function of S100A1 or S100B inhibited chondrocyte differentiation; however, loss of function of either did not appear to significantly affect chondrocyte differentiation, whereas combined loss of function of both proteins enhanced it (Fig 3A,B). This might be due to the functional redundancy between S100A1 and S100B in chondrocyte differentiation, which is supported by previous reports that a single deletion of S100A1 or S100B in mice caused no abnormality in skeletal development or growth (Xiong *et al*, 2000; Du *et al*, 2002).

As the SOX trio provides signals that are sufficient for the induction of permanent cartilage *in vitro* (Ikeda *et al*, 2004),

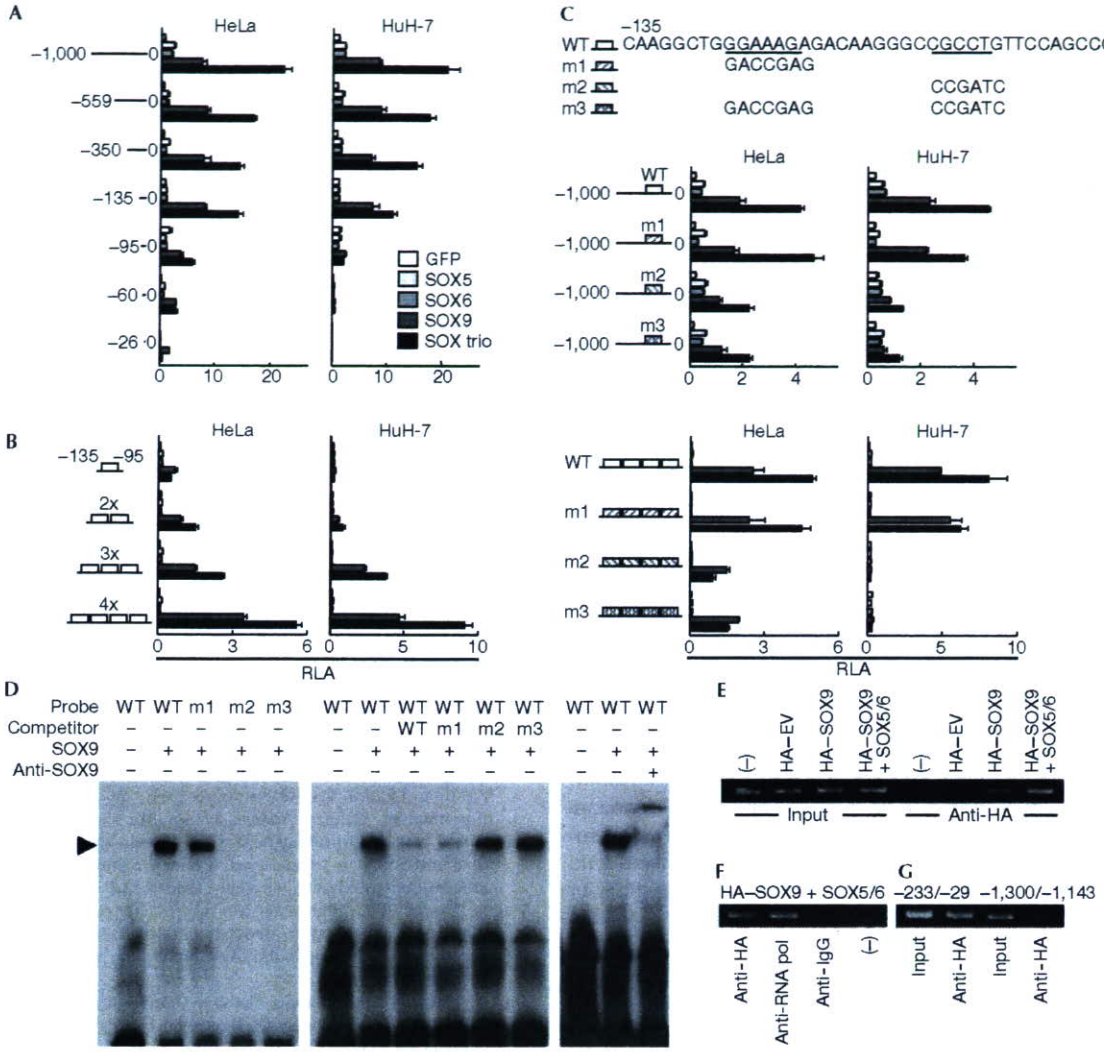

Fig 4 | The SOX trio transcriptionally induces S100A1 through activation of a SOX9 enhancer element in the 5′-end flanking region. (**A**) Deletion analysis using luciferase-reporter constructs containing a 1,000 bp S100A1 5′-end flanking region and the series of deletion fragments in HeLa and HuH-7 cells transfected with green fluorescent protein (GFP), SOX5, SOX6, SOX9 or the SOX trio. (**B**) Dose–response analysis of the tandem repeats of the identified responsive element (−135/−95; A1 box) in the transfected cells. (**C**) Site-directed mutagenesis analysis of either (m1 and m2) or both (m3) of the SOX-binding motifs in the A1 box in the transfected cells. Mutagenesis analysis was performed in the 1,000 bp construct (top) and in the tandem-repeat construct (bottom). (**D**) Electrophoretic mobility shift assay for specific binding of the SOX9 protein with the wild-type (WT) and the mutated (m1, m2 and m3) oligonucleotide probes of the A1 box (left). Cold competition with 50-fold excess of unlabelled WT and mutated probes (middle) is shown. Supershift by a SOX9 antibody of the complex of SOX9 protein and the WT probe is presented. (**E**) Chromatin immunoprecipitation assays for specific binding of SOX9 to the A1 box. Cell lysates of ATDC5 cells transfected with haemagglutinin (HA)-tagged empty vector (HA–EV) or HA-tagged SOX9 in the presence or absence of SOX5 and SOX6 (HA–SOX9 + SOX5/6 or HA–SOX9, respectively) were amplified by a primer set spanning the A1 box (−233/−29) before (input) and after (anti-HA) immunoprecipitation with an HA antibody. (**F**) Immunoprecipitation of lysates of ATDC5 cells transfected with HA–SOX9 and SOX5/6 was carried out using an HA antibody, a positive control RNA polymerase II antibody (anti-RNA pol), a negative control non-immune IgG antibody (anti-IG), or without antibody (-), and amplified with the primer set mentioned above. (**G**) Amplification of lysates of ATDC5 cells transfected with HA–SOX9 and SOX5/6 was carried out using a primer set spanning (−233/−29) or not spanning (−1,300/−1,143) the A1 box, before (input) and after (anti-HA) immunoprecipitation with an HA antibody. The graphs are expressed as means (bars) ± s.d.s (error bars) for 3 wells/group. SOX, sex-determining region Y-type high mobility group box.

understanding of the molecular network related to the SOX–S100 signal will greatly benefit the advancement of cartilage regenerative medicine. Considering that induction of S100A1 and S100B by the SOX trio is not specific to chondrogenic cells (Fig 1), and that both S100 and SOX proteins are expressed in various organs, the SOX–S100 signal might be important in cellular functions other than chondrocyte differentiation in other tissues.

METHODS

Cell cultures. hMSCs, human dermal fibroblasts, HuH-7 and HeLa cells were cultured in high-glucose DMEM with 10% FBS. ATDC5 cells were grown and maintained in DMEM/F12 (1:1) with 5% FBS. To determine early differentiation, the ATDC5 cells cultured in the presence of ITS (insulin, transferrin and sodium selenite) supplement (Sigma, St Louis, MO, USA) for 1 week were stained with 0.1% Alcian blue 8GS (Sigma) in 0.1 M HCl. To induce hypertrophic differentiation and mineralization, ATDC5 cells were cultured in the presence of ITS supplement for 3 weeks and then the medium was replaced by α-MEM/5% FBS with 4 mM inorganic phosphate and cells were grown for 2 days, as described previously (Magne *et al*, 2003). ALP staining was carried out using a solution containing 0.01% naphtol AS-MX phosphate disodium salt, 1% *N,N*-dimethyl-formamide and 0.06% fast blue BB (Sigma). ALP activity was measured with a Lab Assay ALP kit (Wako, Osaka, Japan), according to the manufacturer's instructions. In addition, the cells were stained with 2% Alizarin red S solution.

Immunostaining. Tissues from C57BL6 mouse embryos (embryonic day 17.5) were fixed in 4% paraformaldehyde/PBS overnight at 4 °C, embedded in paraffin and cut into 5 μm sections. Sections were incubated overnight at 4 °C with primary antibodies against S100A1 (1:200; Upstate, Charlottesville, VA, USA), S100B (1:200; Sigma), SOX5, SOX6, SOX9 (1:500; Santa Cruz Biotechnology, Santa Cruz, CA, USA), COL2, COL10 (1:500; LSL), proliferating cell nuclear antigen (1:200; Cell Signaling Technology, Danvers, MA, USA) or non-immune rabbit serum (1:200). The localizations were detected with horseradish peroxidase-conjugated secondary antibodies (Promega, Madison, WI, USA). For immunocytochemistry, ATDC5 cells, which were retrovirally transduced with S100A1 or S100B, were fixed in 4% paraformaldehyde/PBS for 10 min and incubated with the primary antibodies at 25 °C for 1 h. A secondary antibody conjugated with Alexa 488 (Molecular Probes, Eugene, OR, USA) was used for fluorescent visualization and the nucleus was counterstained with Hoechst 33258 (Sigma).

Luciferase assay. The luciferase assay was carried out with a dual-luciferase-reporter assay system (Promega) and a Lumat LB 9507 (Berthold, Bad Wildbad, Germany).

Electrophoretic mobility shift assay. SOX9 protein was prepared by *in vitro* translation using TNT T7 Quick System (Promega) and pCITE4 vector (Novagen, Milwaukee, WI, USA) into which SOX9 complementary DNA was cloned. The translation product was verified by western blotting. EMSA was carried out using a DIG gel shift kit (Roche, Mannheim, Germany) according to the manufacturer's instructions.

Chromatin immunoprecipitation assay. The ChIP assay was carried out with an EZ ChIP kit (Upstate) according to the manufacturer's instructions.

Other experiments. The detailed methods for construction of expression vectors, cell cultures, microarray analysis, real-time RT–PCR, Western blotting, *in situ* hybridization, luciferase assay, EMSA and ChIP assay are described in the supplementary information online.

Supplementary information is available at *EMBO reports* online (http://www.emboreports.org).

ACKNOWLEDGEMENTS

This study was supported by a grant-in-aid for Scientific Research from the Japanese Ministry of Education, Culture, Sports, Science and Technology (nos. 16390430, 17591549 and 18209047).

REFERENCES

Akiyama H, Chaboissier MC, Martin JF, Schedl A, de Crombrugghe B (2002) The transcription factor Sox9 has essential roles in successive steps of the chondrocyte differentiation pathway and is required for expression of Sox5 and Sox6. *Genes Dev* **16:** 2813–2828

Bi W, Huang W, Whitworth DJ, Deng JM, Zhang Z, Behringer RR, de Crombrugghe B (2001) Haploinsufficiency of Sox9 results in defective cartilage primordia and premature skeletal mineralization. *Proc Natl Acad Sci USA* **98:** 6698–6703

Du XJ, Cole TJ, Tenis N, Gao XM, Kontgen F, Kemp BE, Heierhorst J (2002) Impaired cardiac contractility response to hemodynamic stress in S100A1-deficient mice. *Mol Cell Biol* **22:** 2821–2829

Foster JW *et al* (1994) Campomelic dysplasia and autosomal sex reversal caused by mutations in an SRY-related gene. *Nature* **372:** 525–530

Ikeda T, Kamekura S, Mabuchi A, Kou I, Seki S, Takato T, Nakamura K, Kawaguchi H, Ikegawa S, Chung UI (2004) The combination of SOX5, SOX6, and SOX9 (the SOX trio) provides signals sufficient for induction of permanent cartilage. *Arthritis Rheum* **50:** 3561–3573

Lefebvre V, Li P, de Crombrugghe B (1998) A new long form of Sox5 (L-Sox5), Sox6 and Sox9 are coexpressed in chondrogenesis and cooperatively activate the type II collagen gene. *EMBO J* **17:** 5718–5733

Magne D *et al* (2003) Phosphate is a specific signal for ATDC5 chondrocyte maturation and apoptosis-associated mineralization: possible implication of apoptosis in the regulation of endochondral ossification. *J Bone Miner Res* **18:** 1430–1442

Ng LJ, Wheatley S, Muscat GE, Conway-Campbell J, Bowles J, Wright E, Bell DM, Tam PP, Cheah KS, Koopman P (1997) SOX9 binds DNA, activates transcription, and coexpresses with type II collagen during chondrogenesis in the mouse. *Dev Biol* **183:** 108–121

Sekiya I, Tsuji K, Koopman P, Watanabe H, Yamada Y, Shinomiya K, Nifuji A, Noda M (2000) SOX9 enhances aggrecan gene promoter/enhancer activity and is up-regulated by retinoic acid in a cartilage-derived cell line, TC6. *J Biol Chem* **275:** 10738–10744

Smits P, Li P, Mandel J, Zhang Z, Deng JM, Behringer RR, de Crombrugghe B, Lefebvre V (2001) The transcription factors L-Sox5 and Sox6 are essential for cartilage formation. *Dev Cell* **1:** 277–290

Wagner T *et al* (1994) Autosomal sex reversal and campomelic dysplasia are caused by mutations in and around the SRY-related gene SOX9. *Cell* **79:** 1111–1120

Xiong Z, O'Hanlon D, Becker LE, Roder J, MacDonald JF, Marks A (2000) Enhanced calcium transients in glial cells in neonatal cerebellar cultures derived from S100B null mice. *Exp Cell Res* **257:** 281–289

Enhanced wear resistance of modified cross-linked polyethylene by grafting with poly(2-methacryloyloxyethyl phosphorylcholine)

Masayuki Kyomoto,[1] Toru Moro,[2] Tomohiro Konno,[3] Hiroaki Takadama,[4] Noboru Yamawaki,[1] Hiroshi Kawaguchi,[2] Yoshio Takatori,[2] Kozo Nakamura,[2] Kazuhiko Ishihara[3]

[1]*Research and Development Corporate Division, Japan Medical Materials Corporation, Osaka, Japan*
[2]*Department of Orthopaedic Surgery, School of Medicine, The University of Tokyo, Tokyo, Japan*
[3]*Department of Materials Engineering, School of Engineering and Center for NanoBio Integration, The University of Tokyo, Tokyo, Japan*
[4]*Materials Research and Development Laboratory, Japan Fine Ceramics Center, Nagoya, Japan*

Received 17 May 2006; revised 28 September 2006; accepted 28 September 2006
Published online 30 January 2007 in Wiley InterScience (www.interscience.wiley.com). DOI: 10.1002/jbm.a.31134

Abstract: We developed a cross-linked polyethylene (CLPE) modified with a phospholipid polymer in order to address the serious problem of osteolysis caused by wear particles derived from the polyethylene components of artificial hip joints. Our goal of preventing aseptic loosening could be achieved by avoiding any formation of CLPE wear particles or suppressing the activation of cell systems by the wear particles. We investigated the surface and wear resistance properties of 2-methacryloyloxyethyl phosphorylcholine (MPC) polymer grafted onto the surface of CLPE (CLPE-*g*-MPC). The relative density of MPC polymer chains was determined by the P—O group index. Generally, polymerization times correspond to the number of polymer chains in radical polymerization. After 3.0×10^6 cycles in a hip joint simulator test, the steady wear rates of the untreated CLPE and CLPE-*g*-MPC cups with a low P—O group index were as high as 4 mg/10^6 cycles; those of the CLPE-*g*-MPC cups with high P—O group indexes, that is, 0.46 and 0.48, markedly decreased to −1.12 and 0.16 mg/10^6 cycles, respectively. Therefore, the grafting of an MPC polymer with high density would be essential in order to maintain the long-term wear resistance of CLPE-*g*-MPC as an orthopedic bearing material. © 2007 Wiley Periodicals, Inc. J Biomed Mater Res 82A: 10–17, 2007

Key words: joint replacements; polyethylene; phospholipid; phosphorylcholine; wear mechanisms

INTRODUCTION

As the number of aged persons in the world increases year by year, the increase in patients with poorly functioning joints due to external injury or disease is becoming a serious social problem. This means that the quality of artificial joints is becoming increasingly important. Most patients who receive an artificial joint experience a dramatic relief of pain and enjoy a rapid improvement in the quality of life. The most widely used bearing couple for artificial joint systems is the combination of an ultra-high molecular weight polyethylene (UHMWPE) acetabular component and a metal (generally Co-Cr-Mo alloy) femoral component. However, osteolysis caused by wear particles of the UHMWPE is a serious problem with artificial hip joints.[1–3] Reducing wear particle production from UHMWPE is one way of preventing osteolysis. Efforts to decrease these particles have focused on using combinations other than metal-on-UHMWPE and improving the bearing materials themselves.

Several highly cross-linked polyethylenes (CLPE), irradiated with 50–105 kGy, have been launched since 1998 and used extensively.[4,5] Gamma and electron beam irradiation at various doses are used to produce CLPE and numerous *in vitro* studies have been performed using it. In published studies, CLPE subjected to 50–105 kGy exhibited an 80–90% reduc-

Correspondence to: M. Kyomoto, Japan Medical Materials Corporation, Uemura Nissei Bldg. 9F 3-3-31 Miyahara, Yodogawa-Ku, Osaka 532-0003, Japan; e-mail: kyomotom@jmmc.jp

Contract grant sponsor: Japanese Ministry of Education, Culture, Sports, Science, and Technology; contract grant number: 15390449
Contract grant sponsor: Japanese Ministry of Health, Labor, and Welfare

tion in wear rate compared with conventional polyethylene.[6,7] Furthermore, clinical results have confirmed CLPE's effective wear-resistance. However, while the efficacy of the CLPE is evidenced by these reports, *in vivo* the reduction of wear is reported to be only 40–60%.[8–12] Therefore, further improvement of CLPE is desirable.

Recently, we have developed a new-concept artificial hip joint with 2-methacryloyloxyethyl phosphorylcholine (MPC) polymer grafted onto the surface of CLPE (CLPE-*g*-MPC); it has been designed to reduce wear and suppress bone resorption.[13] MPC, a methacrylate monomer with a phospholipid polar group in the side chain, is a novel biomaterial designed and developed by Ishihara et al. that mimics the neutral phospholipids of biomembranes.[14] Various polymers containing MPC units are already widely used as biomaterials.[15,16] The biomembrane-like surface is readily obtained by treating the substrate materials with MPC polymer. The artificial biomembrane surface thus formed exhibits excellent biocompatibility; it is hydrophilic and forms a thin film of free water under physiological conditions.[17] Several medical devices have already been developed utilizing MPC polymer. These devices have been subjected to clinical use with the approval of the Food and Drug Administration of the USA; therefore, the efficacy and safety of the MPC polymer as a biomaterial are well established.[18–20]

We have been developing novel artificial joints with very-low-friction bearing surfaces by combining the biocompatible and hydrophilic MPC polymer with CLPE; this has been accomplished by using a photo-induced radical polymerization technique. This technique facilitates direct grafting of MPC to CLPE, thereby forming C—C covalent bonding between the MPC polymer and CLPE substrate. The advantage of this technique is that the MPC polymer graft occurs only on the CLPE surface and has no effect on the bulk properties of the CLPE substrate. The present study investigated the structure and properties of the MPC polymer layer formed on the CLPE surface by photo-induced radical graft polymerization. The wear-resistant properties of the CLPE-*g*-MPC are discussed in terms of the characteristics of the MPC polymer layer.

MATERIALS AND METHODS

Chemicals

Benzophenone and acetone were purchased from Wako Pure Chemical Industries (Osaka, Japan). 2-Methacryloyloxyethyl phosphorylcholine (MPC) was synthesized industrially using the method reported by Ishihara et al.[14] and was supplied by Ai Bio-Chips Co. (Tokyo, Japan).

MPC graft polymerization

Compression-molded UHMWPE (GUR1020 resin; Poly Hi Solidur, IN) bar stock was γ-irradiated with 50 kGy in N_2 gas and annealed at 120°C for 7.5 h in N_2 gas for cross-linking. The cross-linked polyethylene (CLPE) specimens were machined from this bar stock after cooling. The specimens were immersed in an acetone solution containing 10 mg/mL benzophenone for 30 s and then dried in the dark to remove acetone at room temperature. The amount of benzophenone adsorbed on the surface was determined by ultraviolet spectroscopy to be 3.5×10^{-11} mol/cm^2 using a previously described method.[21] The MPC monomer was dissolved in degassed pure water to a concentration of 0.5 mol/L. The CLPE specimens coated with benzophenone were immersed in the aqueous MPC solution. The photo-induced graft polymerization on the CLPE surface was carried out with ultraviolet irradiation of 5 mW/cm^2 for 10–360 min at 60°C using a Toshiba D-35 filter that permitted the passage of ultraviolet light with a wavelength of 350 ± 50 nm only. After the polymerization, the CLPE-*g*-MPC specimens were removed, washed with pure water and ethanol, and then dried. The CLPE-*g*-MPC specimens were gamma-sterilized with a dose of 25 kGy under N_2 gas.

Surface analysis by using XPS, water-contact angle measurement, and FT-IR/ATR

The surface elemental conditions of the CLPE before and after MPC grafting were analyzed by X-ray photoelectron spectroscopy (XPS). The XPS spectra were obtained using an AXIS-HSi165 spectrophotometer (Kratos Analytical, UK) equipped with an Mg-Kα radiation source at 15 kV at the anode. The take-off angle of the photoelectrons was maintained at 90°. Five scans were taken for each sample.

The static water-contact angle of the CLPE-*g*-MPC with various photo-polymerization periods was measured by a sessile drop method using an optical bench-type contact angle goniometer (Model DM300; Kyowa Interface Science Co., Saitama, Japan). Drops of purified water (1 μL) were deposited onto the surface of the CLPE-*g*-MPC and the contact angles were directly measured with a microscope after each dropping (60 s), according to the ISO 15989 standard.[22] Fifteen replicate measurements were performed on each sample and the contact angle values were averaged.

The functional-group vibrations of the CLPE-*g*-MPC surface with various photo-polymerization periods were examined by Fourier-transform infrared (FT-IR) spectroscopy with attenuated total reflection (ATR) equipment. The measurements were performed over a range of 800–2000 cm^{-1} by using an FT-IR analyzer (Perkin-Elmer FT-IR 1650; Perkin-Elmer Corp., MA) at a resolution of 4.0 cm^{-1} for 100 scans.

The relative amount of grafted MPC polymer unit on the CLPE surface was evaluated by quantification of the phosphate (P—O) group that is contained within the structure of the MPC unit. The relative amount of phosphate

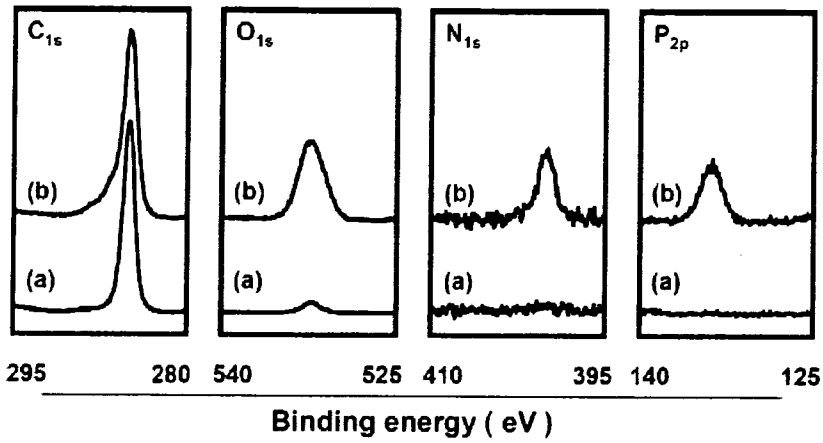

Figure 1. XPS spectra of CLPE-*g*-MPC. (a) CLPE (untreated), (b) CLPE-*g*-MPC.

group was defined as the P—O group index and was calculated as follows.

$$\text{P—O group index} = (1080\ \text{cm}^{-1}\ \text{peak intensity})/(1460\ \text{cm}^{-1}\ \text{peak intensity})$$

Cross-section of CLPE-*g*-MPC observed with TEM

A cross-section of the MPC polymer layer on the CLPE-*g*-MPC surface produced by various photo-polymerization periods was observed with a transmission electron microscope (TEM). The specimens (two pieces for each irradiation time) were first embedded in epoxy resin, stained with ruthenium oxide vapor at room temperature, and then sliced into ultra-thin films (~100-nm thick) by using a Leica Ultra Cut UC microtome (Leica Microsystems, Wetzlar, Germany). A JEM-1010 electron microscope (JEOL, Tokyo, Japan) was used for the TEM observation at an acceleration voltage of 100 kV.

Hip simulation wear test

The inner and outer diameters of the CLPE-*g*-MPC cups used in the hip joint simulator were 26 mm and 52 mm, respectively. For each irradiation time (0, 23, 45, 90, and 180 min) four pieces were prepared. The wear test was performed using a 12-station hip joint simulator (MTS system Corp., MN). A 26-mm Co-Cr-Mo alloy femoral ball component (Japan Medical Materials Corp., Osaka, Japan) was used as an acetabular component. A mixture of 25% bovine serum, 20 m*M*/L of ethylenediaminetetraacetic acid (EDTA), and 0.1% sodium azide was used as lubricant, according to the ISO 14242-1 standard.[23] The lubricant was replaced every 0.5×10^6 cycles. Walks, simulating a physiologic loading curve (Paul-type) with double peaks of 1793 and 2744*N* (183 and 280 kgf) loads, were applied with multidirectional (biaxial and orbital) motion of 1 Hz frequency. The wear was determined by weighing the polyethylene cups. Load-soak controls ($n = 2$) were used to compensate for fluid absorption by the wear specimens.[24] The weights of the cups were measured every 0.5×10^6 cycles. The testing continued until a total of 3.5×10^6 cycles were completed.

To evaluate the net wear, corrected for any influence from plastic deformation, a melt-recovery operation was performed on selected samples of both CLPE and CLPE-*g*-MPC cups after the simulator tests, according to the method of Muratoglu et al.[25] The cups were melted at 150°C in a vacuum and allowed to cool down to the room temperature. The surface features of the bearing surfaces of the cups were observed with a confocal laser scanning microscope (OLS1200; Olympus Corp., Tokyo, Japan).

RESULTS

Figure 1 shows the XPS spectra (C_{1s}, O_{1s}, N_{1s}, and P_{2p}) of CLPE and CLPE-*g*-MPC. In the C_{1s} spectra of both CLPE and CLPE-*g*-MPC a strong peak was observed at 285 eV. This peak is attributed to the carbon atoms in the C—C or C—H groups. In the O_{1s} spectrum of CLPE-*g*-MPC, a significant peak assigned to the C—O group was observed at 532 eV. This peak is mainly ascribed to the MPC units. Even untreated CLPE exhibited a small peak at 532 eV. In this case, the peak is attributed to oxygen atoms and might suggest the contamination and/or oxidation of the CLPE surface. In the N_{1s} and P_{2p} spectra, clear peaks were observed for CLPE-*g*-MPC only. Peaks at 403 and 134 eV were assigned to the $-N^+(CH_3)_3$ and phosphate groups, respectively; these peaks are characteristic of the phosphorylcholine in the MPC units. Table I summarizes the elemental compositions of the surfaces of untreated CLPE and CLPE-*g*-MPC. The measured contents of nitrogen (*N*) and phosphorous (*P*) in the CLPE-*g*-MPC was 5.1 and 5.2, respectively. These values were almost equivalent to the theoretical values ($N = 5.3$, $P = 5.3$) of MPC polymer.

Figure 2 shows the FT-IR/ATR spectra of CLPE and CLPE-*g*-MPC. A transmittance absorption peak was observed at 1460 cm^{-1} for both CLPE and

TABLE I
Surface Elemental Compositions (%) of CLPE (Untreated) and CLPE-*g*-MPC

Samples	C	O	N	P
Untreated CLPE	99.6 (100.0)	0.4 (0.0)	0.0 (0.0)	0.0 (0.0)
CLPE-*g*-MPC	61.8 (57.9)	27.9 (31.6)	5.1 (5.3)	5.2 (5.3)

Theoretical elemental compositions of CLPE and MPC polymer are shown in the parentheses, respectively.

CLPE-*g*-MPC. This peak is attributed mainly to the methylene (CH_2) chain in the CLPE substrate since the peak intensity is very strong and it is unchanged between the CLPE and the CLPE-*g*-MPC. However, the transmittance absorption peaks at 1240, 1080, and 970 cm^{-1} were observed only for the CLPE-*g*-MPC. These peaks are ascribed to the phosphate (P—O) group in the MPC unit. Similarly, the transmittance absorption peak at 1720 cm^{-1} observed for CLPE-*g*-MPC only corresponds to the ketone group in the MPC unit.

The relative P—O group index was calculated from the ratio of the FT-IR peak intensities at 1080 and 1460 cm^{-1} as a measure of the amount of MPC unit grafted onto the CLPE surface; this was done because the peak intensity at 1460 cm^{-1} remains unchanged.

Figure 3 shows the calculated P—O group index as a function of the irradiation time for the CLPE-*g*-MPC specimens. The P—O group index increased as the irradiation time was increased.

Figure 4 shows the static water-contact angle as a function of the calculated P—O group index for the CLPE-*g*-MPC specimens. The static water-contact angle on the untreated CLPE was 88° and decreased markedly with an increase in the P—O group index. When the P—O group index was greater than 0.3, the static water-contact angle became constant at the low value of 15°.

Figure 5 shows cross-sectional TEM images of CLPE-*g*-MPC produced with various ultraviolet irradiation times during polymerization. Lamellae of the order of 100–400 nm in length and 10–20 nm in thickness were observed in the CLPE substrate regardless of irradiation time, and the lamellae were 50–100 nm in length and 5–15 nm in thickness near the surface. With irradiation times longer than

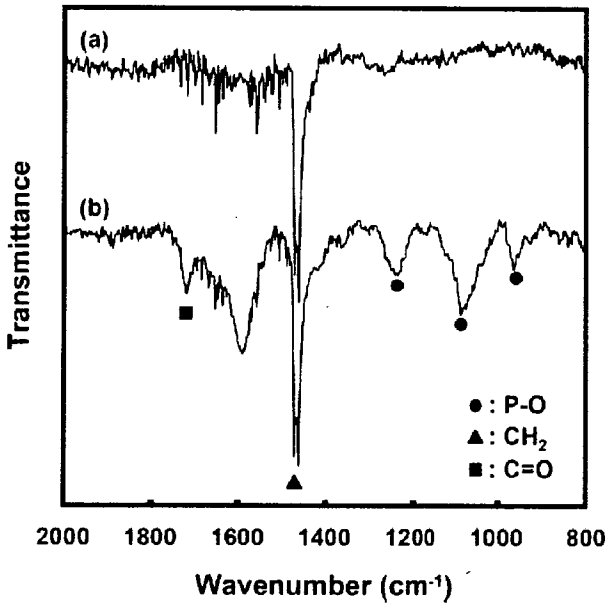

Figure 2. FT-IR/ATR spectra of CLPE-*g*-MPC. (a) CLPE (untreated), (b) CLPE-*g*-MPC.

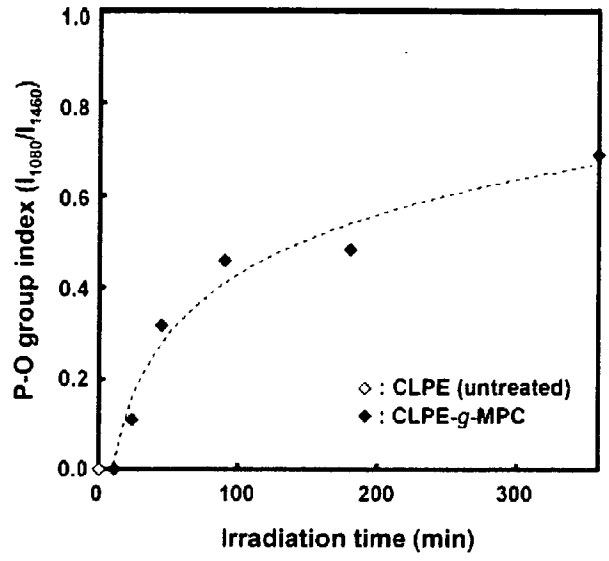

Figure 3. P—O group index as a function of irradiation time for CLPE-*g*-MPC.

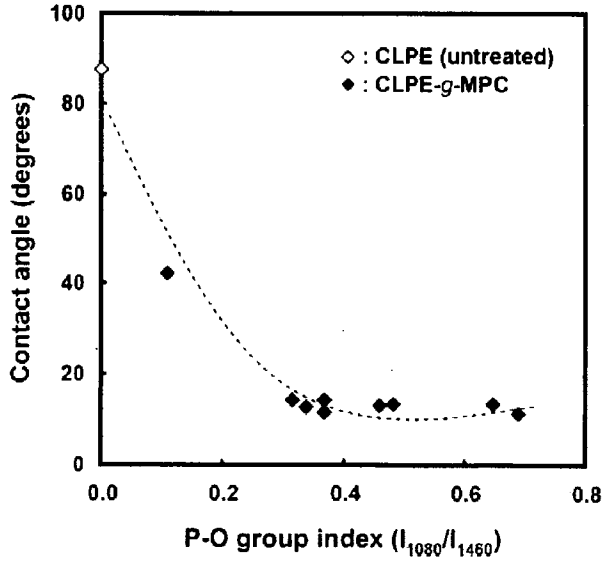

Figure 4. Static water-contact angle as a function of P—O group index for CLPE-*g*-MPC.

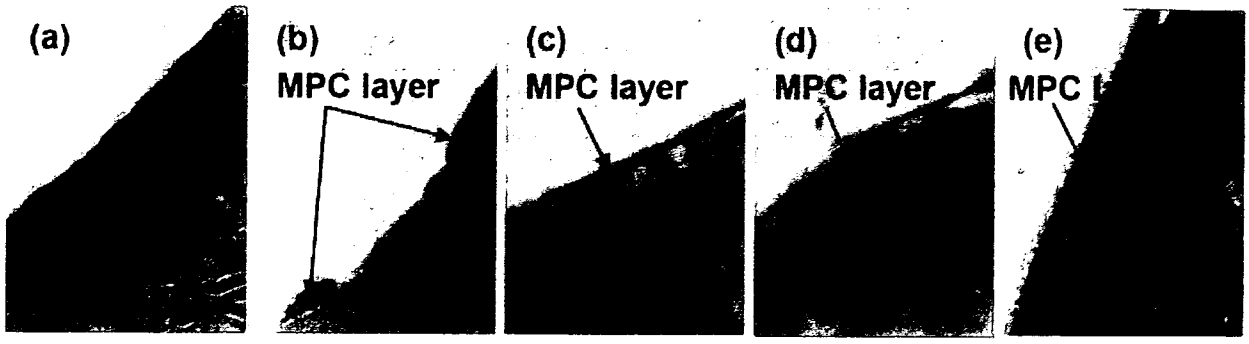

Figure 5. Cross-section TEM images of CLPE-*g*-MPC with various photo-polymerization times. Bar = 200 nm. (a) 11 min, (b) 23 min, (c) 45 min, (d) 90 min, and (e) 180 min.

45 min, a grafted MPC polymer layer 100–200 nm thick was clearly observed on the surface of the CLPE substrate. The MPC-covered region was coexistent with uncovered regions after an irradiation time of 23 min, although the thickness on the MPC polymer layer of the covered region remained the same (100–200 nm). With irradiation for 11 min, no MPC graft layer was observed on the surface of the CLPE. These results indicate that the density of the grafted MPC polymer can be controlled by the polymerization time. This is attributable to the fact that the number of polymer chains produced in a radical polymerization reaction is generally correlated with the photo-irradiation time.

Figure 6 shows the gravimetric wear of CLPE-*g*-MPC with various polymerization irradiation times during the hip joint simulation test. The CLPE-*g*-MPC cups were found to wear significantly less than the untreated CLPE cups. The wear of the CLPE-*g*-MPC cups subjected to 23 min of irradiation started to increase after 2.5×10^6 cycles. Table II shows the wear rate of the CLPE-*g*-MPC cups with various P—O group indexes and irradiation times during the hip joint simulation test. We defined the initial wear rate as that from the start to 0.5×10^6 cycles, and considered the steady wear rate as that from 2.5×10^6 to 3.0×10^6 cycles. All of the untreated CLPE and CLPE-*g*-MPC cups showed low initial wear rates of -1.42 to -3.74 mg/10^6 cycles. The steady wear rate of the untreated CLPE cups and the CLPE-*g*-MPC cups with a low P—O group index of 0.11 increased to 3.68 and 4.64 mg/10^6 cycles, respectively. In contrast, the wear rates of the CLPE-*g*-MPC cups with high P—O group indexes, that is, 0.46 and 0.48, were markedly lower at -1.12 and 0.16 mg/10^6 cycles, respectively.

Figure 7 shows the confocal laser scanning microscopy images of the bearing surfaces of the untreated CLPE and CLPE-*g*-MPC (irradiation time = 90 min) cups before and after the melt-recovery test that was preformed after the simulator test. Before melt-recovery test, scratches were seen in the bearing surfaces of the untreated CLPE and CLPE-*g*-MPC. After melt-recovery test, these scratches completely disappeared from the bearing surfaces. In addition, clear regular circular machining marks were observed on the surface of the CLPE-*g*-MPC, while no marks were observed on the untreated CLPE, indicating that the former was not significantly worn.

DISCUSSION

We have developed an artificial hip joint that uses CLPE-*g*-MPC on the bearing surface; it has been designed to reduce wear and suppress bone resorption. Our previous study reported the effects of graft polymerization of MPC onto the CLPE surface.[13] The MPC grafting markedly decreased the friction and amount of wear. In the present study, we investigated the structure and properties of the MPC polymer layer formed on the CLPE surface by photo-induced

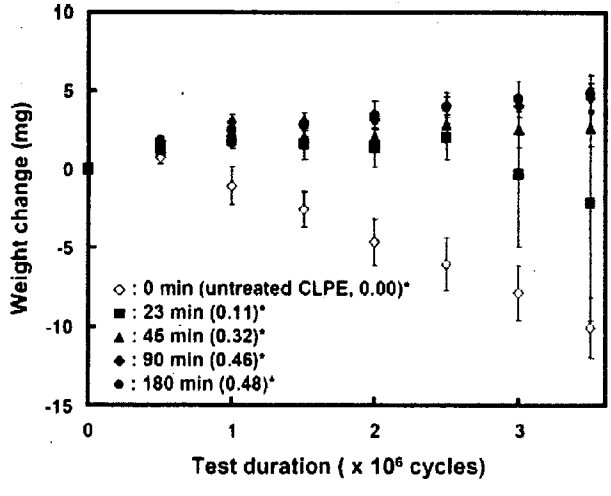

Figure 6. Weight change of CLPE-*g*-MPC cups with various irradiation times during polymerization in the hip joint simulation test. Bars = standard deviations. *P—O group indexes are in parentheses.

TABLE II
Typical P-O Group Index and Wear Rate in Hip Joint Simulator Tests

Irradiation Time (min)	P—O Group Index (I_{1080}/I_{1460})	Initial Wear Rate (mg/10^6 cycles)	Steady Wear Rate (mg/10^6 cycles)
0 (untreated CLPE)	0.00	−1.42 (0.78)	3.68 (0.20)
23	0.11	−2.78 (0.76)	4.64 (6.38)
45	0.32	−2.58 (0.08)	0.68 (0.80)
90	0.46	−3.60 (0.48)	−1.12 (0.32)
180	0.48	−3.74 (0.50)	0.16 (0.08)

The standard deviation is in parentheses.

radical graft polymerization; this report discusses the wear-resistant properties of CLPE-g-MPC in terms of the characteristics of the MPC polymer layer.

After 3.0 × 10^6 cycles of the hip joint simulator test, we confirmed that the CLPE-g-MPC cups with a P—O group index of 0.32 to 0.48 exhibited a relatively low steady wear rate (−1.12 to 0.68 mg/10^6 cycles). This indicates that CLPE-g-MPC cups with a P—O group index greater than 0.32 achieve a >80% reduction in their steady wear rate compared with untreated CLPE as well as CLPE-g-MPC cups with a low P—O group index (0.11) and low density of grafted MPC polymer chains. Since MPC is a highly hydrophilic compound, poly(MPC) is water-soluble. In fact, as shown in Figure 4, the water-wettability of the CLPE-g-MPC surface was considerable greater than that of an untreated CLPE surface. Therefore, the artificial hip joint bearing with the grafted MPC polymer surface exhibited considerably higher lubricity than that without the MPC polymer. The significant reduction in the coefficient of friction of the grafted MPC polymer[13] resulted in a substantial improvement in wear resistance. We assumed that the bearing surface of the artificial hip joint combined with MPC polymer exhibited the fluid film lubrication (or mixed lubrication) of the intermediate hydrated layer; this suggests that this novel artificial hip joint mimics the natural joint cartilage.

It is assumed that several important issues are involved in the long-term retention of the benefits of MPC polymer used in artificial joints under variable and multidirectional loads: strong bonding between the MPC polymer and the CLPE surface, high mobility of the free end groups of the MPC polymer, and a high density of the introduced MPC polymer. These considerations are based on previous studies

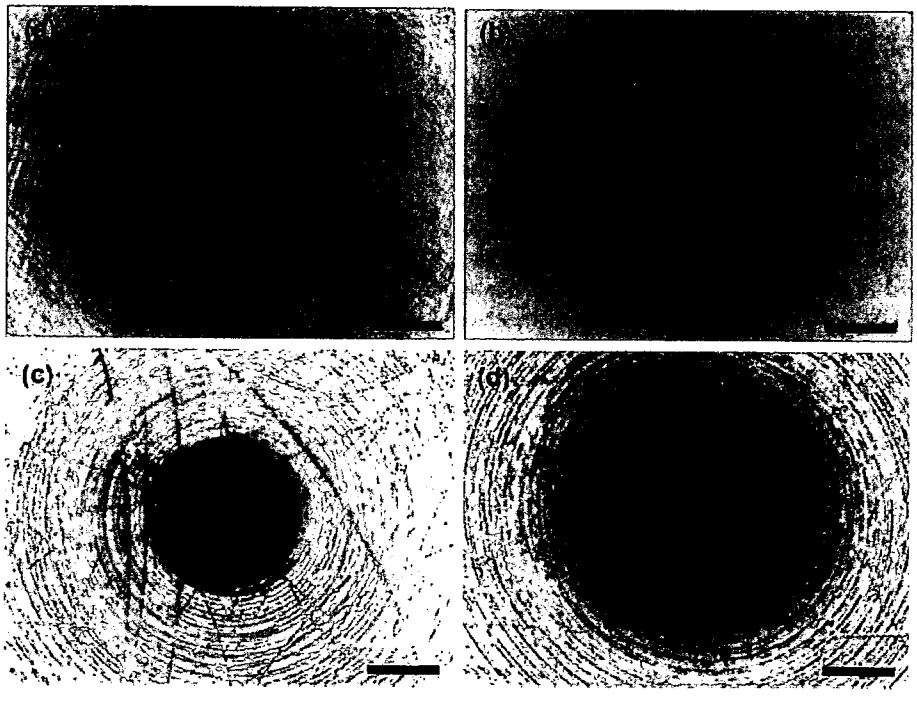

Figure 7. Confocal laser scanning microscope images of the bearing surfaces of the cups before and after a melt-recovery test that was performed after the simulator test. (a) CLPE before melt-recovery test, (b) CLPE after melt-recovery test, (c) CLPE-g-MPC before melt-recovery test, and (d) CLPE-g-MPC after melt-recovery test. Bar = 400 μm.

of charged polymers (polyelectrolytes) reported by Raviv et al.[26,27] With this in mind, we selected photo-induced radical graft polymerization to produce C—C covalent bonding between a carbon atom of CLPE and an end group of the MPC polymer chain. As shown in Figure 5, the crystalline structure of the CLPE substrate is unchanged even after the grafting of MPC, regardless of irradiation time (polymerization time). This indicates that ultraviolet-induced radical graft polymerization does not affect the structure of the CLPE substrate. The unchanged structure of the CLPE substrate itself is very important because the CLPE cup acts not only as a bearing material but also as a structural material in the artificial hip joint. Furthermore, when the MPC layer disappears on the substrate surface, the exposed CLPE substrate may have lower wear than uncross-linked polyethylenes. We therefore deemed that the substrate was CLPE, although it was shielded by the MPC layer. In a previous study using gamma irradiation,[28] the lower-molecular-weight cross-linked GUR1020 materials had higher mechanical properties (tensile and impact properties) for all doses compared to the higher-molecular-weight cross-linked GUR1050 materials. Nevertheless, the cross-linked GUR1020 materials exhibited the same wear rate as the cross-linked GUR1050 materials. Therefore, we selected the GUR1020 compression-molded bar stock as a CLPE substrate.

To obtain an MPC polymer layer with high density, the irradiation time must be controlled.[20] The density of the MPC polymer chains on the surface of the CLPE gradually increased with increasing irradiation time and the entire surface of the CLPE was coated using polymerization times longer than 45 min. As shown in Figure 5, with longer irradiation, the thickness of the MPC polymer layer remained the same (100–200 nm). In the CLPE-*g*-MPC cups with a high surface density of MPC graft chains, the MPC graft chains are assumed to stand up to exhibit a brush like structure.[29,30] It is generally well-known that the reaction rate of radical polymerization is extremely high.[31] The molecular weight of grafted polymer is therefore controlled by monomer concentration. When the MPC polymer layer has brush like structure, the layer thickness might depend on the molecular weight of grafted MPC polymer. On the other hand, Figure 4 implies that the density of the MPC polymer chains on the surface of the CLPE was different, even if the water-wettability of the CLPE-*g*-MPC was constant (as low as 15°); this is because the P—O group index changed remarkably within the range of 0.3 and 0.7.

As mentioned above, the steady wear rate of CLPE-*g*-MPC cups with a high P—O group index was relatively low even after 3.5×10^6 cycles in the simulator test. As shown in Figure 7, clear machining marks with regular circles remained on the surface of CLPE-*g*-MPC cups even after the simulator test. In other words, the CLPE-*g*-MPC cups were virtually unworn, which is consistent with the relatively low wear observed in the hip joint simulator tests.

Table II shows that several CLPE-*g*-MPC cups exhibited a slight increase in weight (wear rate was negative); this was attributable to slightly enhanced fluid absorption over and above the fluid absorption by the load-soak controls. When using the gravimetric method, we corrected the weight loss for the fluid absorption by subtracting the weight gain that occurred in the load-soak controls. Since the wear cups are subjected to motion and load, there are limitations to this correction; therefore, they are observed to absorb slightly more fluid than their load-soak controls. However, as a result, the correction for fluid absorption by using the load-soak controls data as the correction factor leads to a slight underestimation of the actual weight loss.

The excellent functions of CLPE-*g*-MPC could avoid the activation of cell systems by the wear particles, thus entirely preventing periprosthetic osteolysis and subsequent aseptic loosening.[13] In view of its superior mechanical and biological advantages, the CLPE-*g*-MPC is widely expected to be the next-generation bearing material for artificial hip joints. Arrangements are now being made for the conduction of clinical trials.

In this study, we investigated the surface physical properties of CLPE-*g*-MPC. After a hip joint simulator test, we confirmed that CLPE-*g*-MPC cups with a high surface density of MPC graft chains exhibited a relatively low and steady wear rate. When compared with cups with untreated CLPE and those with CLPE-*g*-MPC with a low P—O group index (cups with low density of grafted MPC polymer chain), these CLPE-*g*-MPC cups exhibited an 80% reduction in their steady wear rate. Thus, it appears that CLPE-*g*-MPC markedly reduces the generation of wear particles. However, the grafting of MPC polymer at a high density is essential to maintain the wear-resistance of CLPE-*g*-MPC as an orthopedic bearing material over long periods of time. We conclude that grafting MPC onto CLPE is a useful method for maintaining efficient lubrication of artificial hip joints over a long period.

The authors thank Dr. Fumiaki Miyaji, Mr. Yoshiki Ando, and Mr. Takatoshi Miyashita (Japan Medical Materials Corp., Osaka, Japan) for their excellent technical assistance.

References

1. Harris WH. The problem is osteolysis. Clin Orthop 1995;311:46–53.

2. Kobayashi A, Freeman MA, Bonfield W, Kadoya Y, Yamac T, Al-Saffar N, Scott G, Revell PA. Number of polyethylene particles and osteolysis in total joint replacements. A quantitative study using a tissue-digestion method. J Bone Joint Surg Br 1997; 79:844–848.
3. Sochart DH. Relationship of acetabular wear to osteolysis and loosening in total hip arthroplasty. Clin Orthop 1999;363: 135–150.
4. Collier JP, Currier BH, Kennedy FE, Currier JH, Timmins GS, Jackson SK, Brewer RL. Comparison of cross-linked polyethylene materials for orthopaedic applications. Clin Orthop Relat Res 2003;414:299–304.
5. Muratoglu OK, Mark A, Vittetoe DA, Harris WH, Rubash HE. Polyethylene damage in total knees and use of highly crosslinked polyethylene. J Bone Joint Surg Am 2003;85:S7–S13.
6. McKellop H, Shen FW, Lu B, Campbell P, Salovey R. Development of an extremely wear-resistant ultra high molecular weight polyethylene for total hip replacements. J Orthop Res 1999;17:157–167.
7. Muratoglu OK, Bragdon CR, O'Connor DO, Jasty M, Harris WH. A novel method of crosslinking ultra-high-molecular-weight polyethylene to improve wear, reduce oxidation, and retain mechanical properties. Recipient of the 1999 HAP Paul Award. J Arthroplasty 2001;16:149–160.
8. Manning DW, Chiang PP, Martell JM, Galante JO, Harris WH. In vivo comparative wear study of traditional and highly cross-linked polyethylene in total hip arthroplasty. J Arthroplasty 2005;20:880–886.
9. Digas G, Kärrholm J, Thanner J, Malchau H, Herberts P. Highly cross-linked polyethylene in cemented THA. Clin Orthop Relat Res 2003;417:126–138.
10. Heicel C, Silva M, dela Rosa MA, Schmalzried TP. Short-term in vivo wear of cross-linked polyethylene. J Bone Joint Surg Am 2004;86:748–751.
11. Martell JM, Verner JJ, Incavo SJ. Clinical performance of a highly cross-linked polyethylene at two years in total hip arthroplasty: A randomized prospective trial. J Arthroplasty 2003;18:55–59.
12. Oonishi H, Kim SC, Takao Y, Kyomoto M, Iwamoto M, Ueno M. Wear of highly cross-linked polyethylene acetabular cup in Japan. J Arthroplasty 2006;18:944–949.
13. Moro T, Takatori Y, Ishihara K, Konno T, Takigawa Y, Matsushita T, Chung UI, Nakamura K, Kawaguchi H. Surface grafting of artificial joints with a biocompatible polymer for preventing periprosthetic osteolysis. Nat Mater 2004;3:829–837.
14. Ishihara K, Ueda T, Nakabayashi N. Preparation of phospholipid polymers and their properties as polymer hydrogel membranes. Polym J 1990;22:355–360.
15. Ishihara K, Aragaki R, Ueda T, Watanabe A, Nakabayashi N. Reduced thrombogenicity of polymers having phospholipid polar groups. J Biomed Mater Res 1990;24:1069–1077.
16. Ishihara K, Ziats NP, Tierney BP, Nakabayashi N, Anderson JM. Protein adsorption from human plasma is reduced on phospholipids polymers. J Biomed Mater Res 1991;25:1397–1407.
17. Kitano H, Imai M, Mori T, Gemmei-Ide M, Yokoyama Y, Ishihara K. Structure of water in the vicinity of phospholipid analogue copolymers as studied by vibrational spectroscopy. Langmuir 2003;19:10260–10266.
18. Kuiper KJ, Nordrehaug JE. Early mobilization after protamine reversal of heparin following implantation of phosphorylcholine-coated stents in totally occluded coronary arteries. Am J Cardiol 2000;85:698–702.
19. Galli M, Sommariva L, Prati F, Zerboni S, Politi A, Bonatti R, Mameli S, Butti E, Pagano A, Ferrari G. Acute and mid-term results of phosphorylcholine-coated stents in primary coronary stenting for acute myocardial infarction. Catheter Cardiovasc Interv 2001;53:182–187.
20. Lewis AL, Tolhurst LA, Stratford PW. Analysis of a phosphorylcholine-based polymer coating on a coronary stent pre- and post-implantation. Biomaterials 2002;23:1697–1706.
21. Ishihara K, Iwasaki Y, Ebihara S, Shindo Y, Nakabayashi N. Photoinduced graft polymerization of 2-methacryloyloxyethyl phosphorylcholine on polyethylene membrane surface for obtaining blood cell adhesion resistance. Colloids Surf B 2000; 18:325–335.
22. ISO. Plastics—Film and sheeting—Measurement of water-contact angle of corona-treated films. 2004. International Organization for Standardization 15989.
23. ISO. Implants for surgery: Wear of total hip-joint prostheses, Part 1: Loading and displacement parameters for wear-testing machines and corresponding environmental conditions for test. 2002. International Organization for Standardization 14242-1.
24. ISO. Implants for surgery: Wear of total hip-joint prostheses, Part 2: Methods of measurement. 2000. International Organization for Standardization 14242-2.
25. Muratoglu OK, Greenbaum ES, Bragdon CR, Jasty M, Freiberg AA, Harris WH. Surface analysis of early retrieved acetabular polyethylene liners: A comparison of conventional and highly crosslinked polyethylenes. J Arthroplasty 2004;19: 68–77.
26. Raviv U, Frey J, Sak R, Laurat P, Tadmor R, Klein J. Properties and interactions of physigrafted end-functionalized poly (ethylene glycol) layers. Langmuir 2002;18:7482–7495.
27. Raviv U, Glasson S, Kampf N, Gohy JF, Jérôme R, Klein J. Lubrication by charged polymers. Nature 2003;425:163–165.
28. Greer KW, King RS, Chan FW. The effects of raw material, irradiation dose, and irradiation source on crosslinking of UHMWPE. In: Kurtz SM, Gsell RA, Martell J, editors. Crosslinked and Thermally Treated Ultra-High Molecular Weight Polyethylene for Joint Replacements. West Conshohoken: American Society for Testing and Materials; 2003. pp 209–220.
29. Matsuda T, Kaneko M, Ge S. Quasi-living surface graft polymerization with phosphorylcholine group(s) at the terminal end. Biomaterials 2003;24:4507–4515.
30. Goda T, Konno T, Takai M, Moro T, Ishihara K. Biomimetic phosphorylcholine polymer grafting from polydimethylsiloxane surface using photo-induced polymerization. Biomaterials 2006;27:5151–5160.
31. Feng W, Brash J, Zhu S. Atom-transfer radical grafting polymerization of 2-methacryloyloxyethyl phosphorylcholine from silicon wafer surface. J Polym Sci Part A: Polym Chem 2004;42: 2931–2942.